EES Catalysis

REVIEW ARTICLE

View Article Online
View Journal | View Issue

Cite this: *EES Catal.*, 2023, **1**, 810

Metal-doped carbon nitride: an all-in-one photocatalyst

Yamei Pang,† Pengfei Li,† Xiaobao Ma,† Lu Sun,† Yichang Liu, † Dan Qu,† Li An*† and Zaicheng Sun *†

As a typical photocatalyst, graphitic carbon nitride (CN) has received significant attention in the field of energy conversion. Its excellent performance is mainly due to its good chemical stability, low cost, and unique framework structure. However, it is still facing some problems demanding prompt solutions, such as insufficient light absorption, rapid recombination of charge carriers, and absence of reactive sites, which lead to an unsatisfactory photocatalytic performance. Therefore, great efforts have been made to solve these issues. Metal doping is treated as a common strategy to prepare modified CN. A large number of studies have shown that metal-doped CN exhibits an improved photocatalytic performance. It not only promotes charge separation but also incorporates reactive sites and raises the reactive selectivity. As a consequence, metal-doped CN can be considered an all-in-one photocatalyst because it combines the photocatalyst and cocatalyst in one unit. This greatly enhances the charge separation efficiency and utilization, resulting in a high photocatalytic performance. Here, the recent progress of metal-doped CN photocatalysts is summarized according to the location of the metal element in the periodic table. The structure–activity relationship of metal atoms on CN is discussed for photocatalytic H_2 production, H_2O_2 production, CO_2 reduction, and other fields. Dual-atom doped CN turns out to be a more active field due to it providing more active sites to alter catalytic pathways and break the linear relationship. Finally, the intrinsic properties of catalysts *e.g.* stability and toxicity are summarized in this review.

Received 4th June 2023,
Accepted 31st July 2023

DOI: 10.1039/d3ey00123g

rsc.li/eescatalysis

Broader context

Photocatalysis is an effective approach to achieving solar to chemical energy conversion. The photocatalyst is the core element to determine light absorption and charge separation. The cocatalyst, which promotes charge separation and adsorbs the substance, is a necessary auxiliary unit to complete the whole photocatalysis process. Developing highly efficient photocatalysts is expected to satisfy the demands for increasing energy consumption and solving environmental pollution issues. Graphitic carbon nitride (CN) has been an important photocatalyst since it was rediscovered in 2009. However, rapid charge recombination results in a low photocatalytic efficiency. Metal doping not only changes the surface chemical structure but also affects the electron distribution of the CN framework, thus leading to the improvement of photocatalytic properties. On the other hand, transition metals are extensively used as active catalytic sites due to their unique d orbital electron configuration. When the metal elements in the d, ds and p regions of the periodic table work as cocatalysts in the photocatalysis system, in this case, the photocatalyst integrates all the functions of light absorption, charge separation and cocatalyst within a single unit. It is named the all-in-one photocatalyst. The photogenerated electron is usually transferred to the metal doping site. The hole is left at the CN framework to form spatial charge separation. The electron can be further passed to the adsorbed species like, protons CO_2, O_2 or N_2 molecules for the reduction reaction. Overall, the photocatalytic performance is continuously improved by doping atoms. It is not only used for the typical hydrogen evolution reaction (HER), CO_2 reduction reaction (CO_2RR), oxygen reduction reaction (ORR), and N_2 reduction reaction (NRR), but also opens a door for photocatalytic organic synthesis.

1 Introduction

Carbon nitride photocatalysts (CN) are widely used in photocatalysis due to their suitable band gap (E_g = ~2.7 eV), visible light response, super chemical/thermal stability, and a simple preparation process.[1,2] CN was first applied to the study of hydrogen production by photocatalytic water splitting by Wang *et al.* in 2009.[3] Since then, researchers have intensified their

---

Center of Excellence for Environmental Safety and Biological Effects, Beijing Key Laboratory for Green Catalysis and Separation, Department of Chemistry, Beijing University of Technology, 100 Pingleyuan, Beijing, 100124, China. E-mail: sunzc@bjut.edu.cn

† These authors contributed equally to this work.

research on using CN in photocatalysis. However, it still suffers from the problems of insufficient light absorption, easy recombination of photogenerated carriers, and a low surface reaction rate,[4–7] which leads to its unsatisfactory photocatalytic performance. Various modifications have been attempted to enhance the photocatalytic performance in the HER,[8] OER,[9] overall water splitting,[10] CO_2 reduction,[11] H_2O_2 production,[12] nitrogen reduction,[13] photocatalytic organic reactions,[14] *etc.*

The modification of CN can be classified into the following categories: (1) morphology modification,[15,16] (2) construction of heterojunctions,[17–20] and (3) doping. By modifying the morphology of CN, it is possible to increase the material's specific area and obtain more reactive sites. The construction of a heterojunction can also improve the photocatalytic activity. CN is combined with different semiconductor materials to form a heterogeneous structure. It is considered to be one of the most feasible strategies to improve the separation efficiency of electron–hole pairs. Doping also includes small molecule doping,[21–25] non-metal element doping,[26,27] metal element doping,[28] *etc.* Ao *et al.* summarized modified CN materials with intramolecular D–A structures formed by small molecular modification. The generated D–A structures extend the π conjugated system effectively and optimize the electronic structure of CN, ultimately improving the photocatalytic performance.[29] Yang *et al.* summarized the recent progress of non-metal modified CN systematically. Non-metallic element doping can reduce the band gap of CN and enhance the light absorption capacity, thus effectively improving the catalytic performance.[30] Fortunately, the above strategies can improve the performance of photocatalysts. A large number of studies have shown that metal-modified CN-based photocatalysts exhibit improved performance. For example, they can promote charge transport, construct rich active sites, and improve the selectivity of catalytic reactions.

In this review, we focus on the preparation of metal-atom doped CN-based materials, the role of the single/dual-metal-atom as the active site, and the applications in photocatalytic H_2, H_2O_2 production, and photocatalytic CO_2 reduction (Fig. 1). First, the alkali metal elements located in the IA group regulate the electron distribution of the system by incorporating alkali metal halides (metal cations) into CN. Second, transition metal elements in the d and ds regions are more integrated into the CN as active sites. Due to their high atomic economy and unique selectivity, single-atom catalysts (SACs) are also a new star. As a typical photocatalyst, the carbon nitride material is an excellent single-atom support. By loading single atoms on carbon nitride, the single atoms can become active sites, *i.e.*, co-catalysts in photocatalytic systems. Transition metal elements act as potential centers of activity that can work as co-catalysts when introduced to carbon nitride. The co-catalyst can be chemically bonded to the photocatalyst to increase the charge transport rate and obtain an all-in-one photocatalyst. Therefore, single-atom doping is of great significance in the field of photocatalysis. In addition, compared with single-atom catalysts, diatomic metals can be used as bifunctional active

Yamei Pang

Yamei Pang is a master's student at Beijing Key Laboratory for Green Catalysis and Separation, Department of Chemistry and Chemical Engineering, Beijing University of Technology. Her current research interests focus on the construction of a modified carbon nitride photocatalyst and the study of photocatalytic performance.

Li An

Li An has been an associate professor of chemistry at Beijing University of Technology, China, since 2019. She received her Master's degree in Physical Chemistry from Beijing University of Technology in 2012 and her PhD degree from Peking University in 2016. Her main research interest is focused on electrocatalysis of proton exchange membrane fuel cells and other materials applied in energy storage devices. An can be reached by email at 08131@bjut.edu.cn.

Zaicheng Sun

Zaicheng Sun received his PhD degree in Chemistry from Changchun Institute of Applied Chemistry, CAS. After that, he started to work as an AvH research fellow at Marburg University in Germany. Followed by a research associate position at UW, Udel, and UNM. He took the professor position at Changchun Institute of Optics, Fine Mechanics and Physics, CAS in 2010. He is currently a professor in the Department of Chemistry and Biology, Beijing University of Technology. His research focuses on the rational design of photocatalysts with high charge separation efficiency and fluorescent carbon dots with tunable emission and their applications.

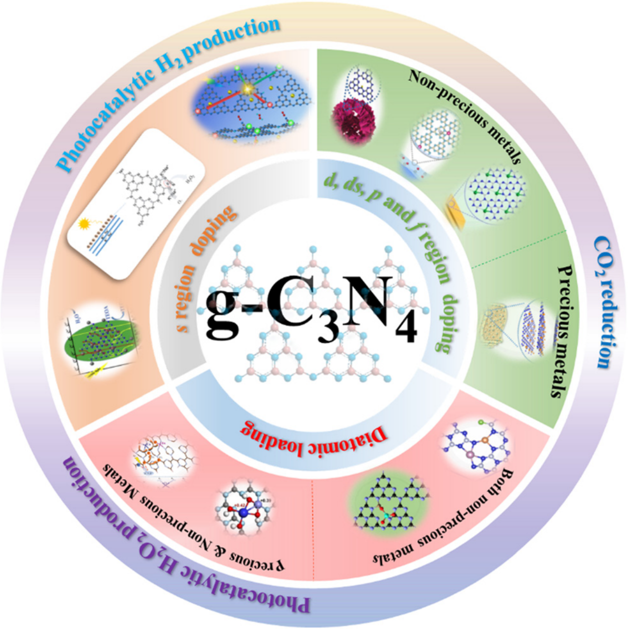

Fig. 1 Metal-doped CN-based photocatalyst and its applications.

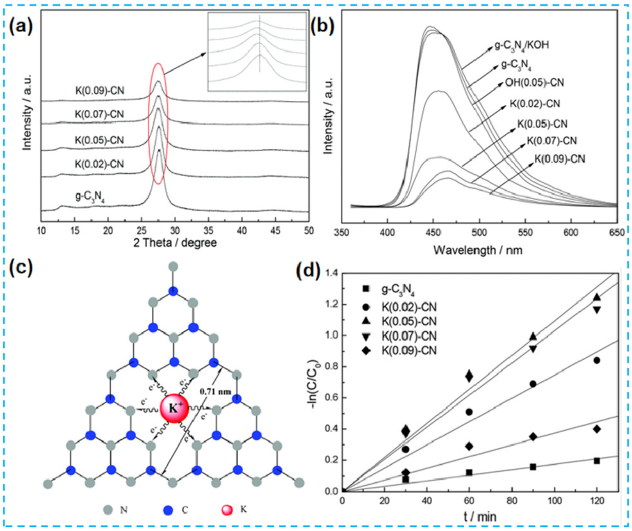

Fig. 2 (a) XRD patterns of the as-prepared CN and K(*x*)-CN. (b) PL spectra of the as-prepared CN-based catalysts. (c) Possible doping site for K ions in K(*x*)-CN. (d) The degradation of RhB under visible-light irradiation.[31]

centers after doping, and the synergistic effect of diatomic co-catalysts is more conducive to the photocatalytic reactions, which is expected to develop into an essential technology for green energy conversion and sustainable development. Finally, the prospect of single/dual-metal atom-modified CN-based photocatalysts is presented. This work guides the preparation of efficient atom-anchored CN-based photocatalysts and their industrial applications.

2 s Region element doping

Numerous previous studies indicate that the doping of alkaline metals can modulate the structure of the energy bands of semiconductor photocatalysts.[5] In 2015, Hu *et al.* reported alkali metal-doped CN photocatalysts in two ways. In the first method, dicyandiamide is used as the CN precursor, and KOH is used as the K source, and the two are mixed thoroughly and then thermally polymerized. In the second method, the pre-synthesized CN is dispersed in a KOH solution to remove water by heating and stirring only. Comparing these two catalysts, K species were present mainly on the CN surface for the materials synthesized by post-treatment of CN with alkali, and the PL intensity did not decrease. This method did not enhance the photogenerated carrier efficiency (Fig. 2b). In the case of the materials synthesized by direct pyrolysis of precursors (K-CN), the doping of potassium would obstruct the growth of CN crystals (Fig. 2a), thus increasing the BET surface area and favouring the adsorption and desorption of reactants and products. During the thermal condensation process, K is doped into the CN lattice through K–N bonds (Fig. 2c). Since the ionic radius of K is more significant than that of C and N, substitution doping occurs but interstitial doping of K would not occur. The interstitial doping increases the interlayer spacing of CN. UV-vis absorption spectra demonstrate that the doping of K changes the energy band structure and thus enhances the mineralization ability of organic pollutants (Fig. 2d).[31]

The above work found that the direct thermal polymerization of alkali metal sources with CN precursors can enhance the photocatalytic performance. In most cases, researchers often chose the alkali metal halide as the metal source, *i.e.*, the molten salt synthesis route. The doping of alkali metal can modify the electronic coupling between CN layers by charge transfer, generation of defect states,[32] and construction of built-in electric fields,[26] which significantly impact the electronic behaviour. In 2018, Chen *et al.* doped K into CN by thermal polymerization of thiourea with KBr (Fig. 3a). Since K ions have a large diameter, the doping of K will enhance the interaction

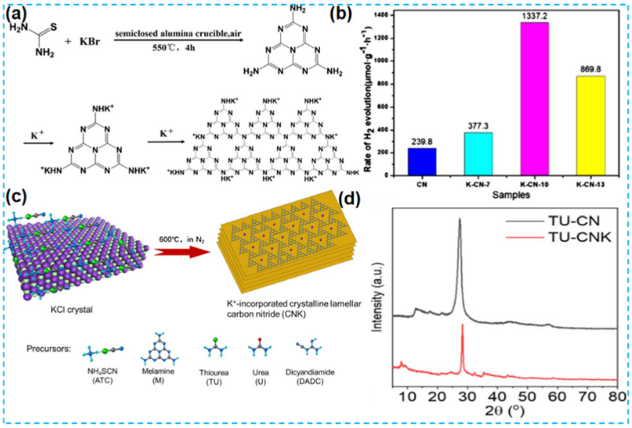

Fig. 3 (a) A possible synthetic mechanism of K-CN-X. (b) Photocatalytic activity of K-doped CN toward the HER from water.[33] (c) Synthesis of CNK frameworks (ATC-CNK, M-CNK, TU-CNK, U-CNK, and DCDA-CNK) on KCl crystals. (d) X-ray diffraction profiles of ATC-CN and ATC-CNK.[34]

with CN nanosheets (and will form N–K bonds) and the vigorous exchange will extend the conjugated system. That is treated as the fundamental reason for enhancing the photocatalytic performance. However, too much KBr will lead to the polymerization of K on the catalyst surface, and some active sites will be blocked, leading to a performance decrease (Fig. 3b).[33] In 2023, a series of CN precursors were thermally polymerized with KCl to form K^+-doped layered CN materials by Zhao *et al.* (Fig. 3c). The doping of K revealed a reduction in the interlayer stacking spacing (002 crystal plane diffraction peaks shifted toward large angles), which demonstrated enhanced interactions and facilitated exciton dissociation (Fig. 3d); XPS characterization revealed the introduction of cyano during thermal polymerization with the K source, which was formed due to incomplete condensation of the CN precursors.[34] Kang *et al.* chose melamine as a precursor and thermally polymerized it directly with KCl/NaCl. The greater the mass of eutectic salt, the more the intensity of both extraordinary diffraction peaks of XRD decreases, which indicates that it affects the growth of CN crystals (Fig. 4a). XPS shows that K^+ and Na^+ are attached to CN through N; it also proves that substitution doping of alkali metals should not occur.[35] Rubidium (Rb), which has similar physical and chemical properties to K, is more reactive and would theoretically provide more Lewis acid–base sites. Therefore, Du *et al.* synthesized CNR by thermally polymerizing dicyandiamide (DCDA) with RbCl salts. The doping of Rb generated cyanide at the end of the triazine ring to inhibit CN polymerization, increased the specific surface area and provided abundant active sites. The doping of Rb^+ with the presence of cyano functional groups (Fig. 4b) enhanced the light absorption of the material and promoted charge separation, which was ultimately beneficial for the photocatalytic H_2O_2 production performance (Fig. 4c).[36]

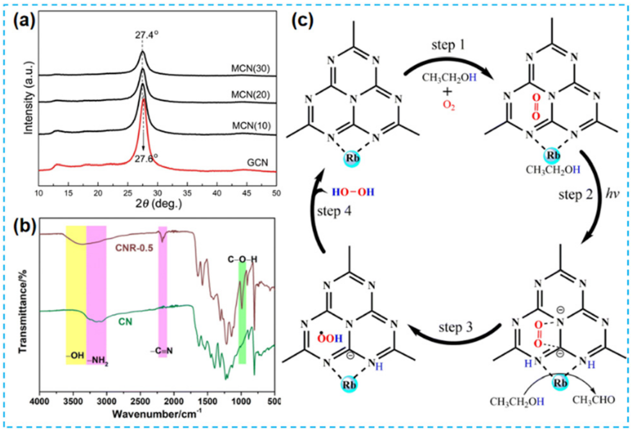

Fig. 4 (a) XRD patterns of K^+–Na^+ codoped CN.[35] (b) FT-IR of CN and Rb doped CN (CNR-0.5). (c) Proposed mechanism of the two-step single-electron O_2 reduction reaction pathways on CNR-0.5.[36]

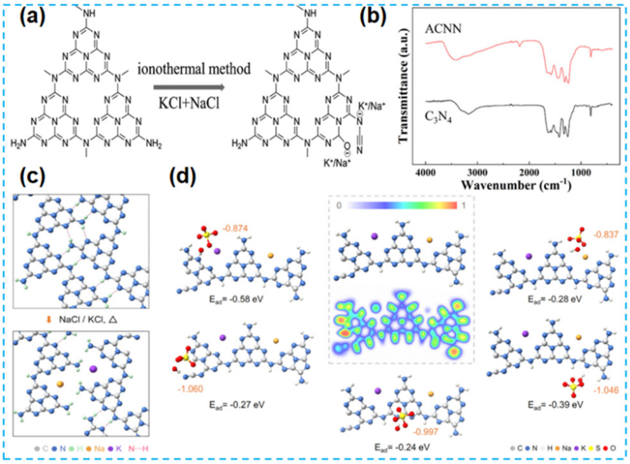

Fig. 5 (a) Schematic illustration of the procedure for introducing alkali metal dopants and N vacancies on CN. (b) FTIR spectra of ACNN (alkali metal dopants and N vacancies on CN) and CN.[37] (c) Proposed structure evolution of PCN during the thermal treatment process in alkali metal salts. (d) Color-filled map of calculated ELF of ACN (alkali metal salts modified carbon nitride).[38]

Would the photocatalytic performance be improved if the molten eutectic salt was further heat-treated on the prepared CN by the second method of Hu *et al.*? In 2020, Quan *et al.* obtained CN powder by pyrolysis of the urea with NaCl/KCl under an argon atmosphere and the metal salts were removed by washing with deionized water. Finally, the alkali metal-doped CN materials were obtained (Fig. 5a). The eutectic salt corrodes at high temperatures, and the surface of the CN-based material becomes rough. The infrared mapping reveals the presence of cyano, a functional group (Fig. 5b). The coordination of alkali metal with N/O enhances the interlayer interaction, which is more favourable for electron transfer to CN. Characterization results prove that the doping of alkali metal can improve the charge separation efficiency, change the energy band structure, and improve the light absorption ability, thus enhancing the ability of H_2O_2 production.[37] In 2022, Guo *et al.* synthesized modified materials under a nitrogen atmosphere using the same method as above (Fig. 5c). Lone pairs of electrons on Na and K, and N atoms formed stable chemical coordination, leading to the disruption of the hydrogen bonding of the structure and the creation of a large number of defects (cyano and N vacancies). This modification strategy facilitates electron transfer. The materials have a more comprehensive light absorption range and lower electron leap energy barriers (Fig. 5d), enhancing photocatalytic efficiency.[38]

In the above synthesizing route, we found two main synthetic strategies for alkali metal doping, direct thermal polymerization of alkali metal salts and CN precursors, and post-treatment of the synthesized CN. The second method has a better catalytic performance than the first method. In short, the introduction of alkali metal affects the structure of CN. The introduction of alkali metal will result in a cyano group in the CN framework. Alkali metal and N will create coordination sites. These structural changes will determine the properties of the catalyst. The introduction of alkali metal ions and the presence of cyanide enhance the interaction between CN layers, broaden the visible light absorption range of CN, and improve the photogenerated carrier separation efficiency. These are practical pieces of evidence that the photocatalytic performance can be significantly enhanced.

3 d Region and ds region element doping

Regarding the design of modified CN materials, loaded co-catalysts have proven to be an effective way to prepare efficient photocatalysts.[39] Elements in different regions have different electron configurations, which can strongly alter the properties of the CN. In 2011, Zhang's group successfully prepared Fe-based single-atom catalysts by introducing single-atom sites. Later, single-atom motivations have become a popular research topic in this field.[40] Carbon nitride is an excellent single atom carrier. When the single atom is introduced into the CN structure, the single atom can become the catalytic active site to play the role of co-catalyst. In this design, the co-catalyst is chemically bonded to the photocatalyst by a chemical bond to improve charge transport efficiency, so it turns into an all-in-one catalyst, which has important significance in photocatalysis.

3.1 Noble metal doping

In the preparation of the catalyst, it is found that most noble metals can be used as catalysts for the surface reaction. In practical applications, platinum (Pt), rhodium (Rh), silver (Ag), ruthenium (Ru), and so on are commonly used; in particular, platinum (Pt) and rhodium (Rh) are the most widely used. This mainly depends on their d electron orbitals not filling and the surface being accessible to adsorption reactants. Moderate strength, conducive to forming intermediate "active compounds", has high catalytic activity. In addition, it has high-temperature resistance, oxidation resistance, corrosion resistance, and other comprehensive excellent characteristics. Therefore, it has become an essential catalytic material. Considering the high cost of noble metals, reducing the size of noble metal clusters to the state of single atoms can maximize the atomic utilization of noble metals.[41] Therefore, it is an effective strategy to dope noble metal single atoms on CN to improve catalyst activity.

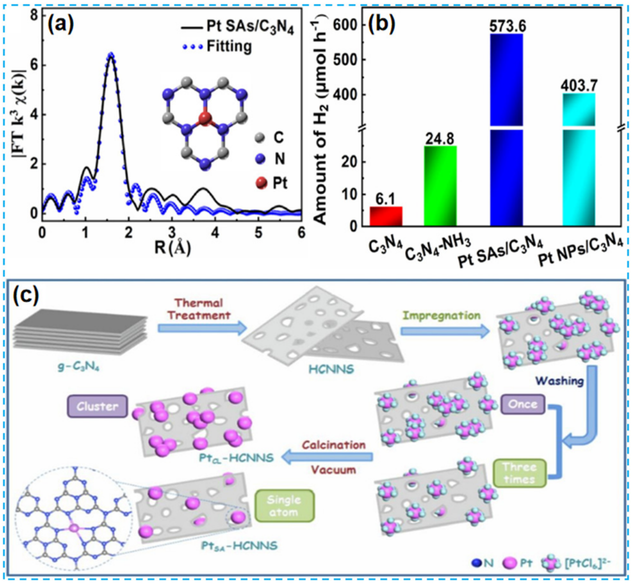

Fig. 6 (a) EXAFS fitting Pt curve for Pt SAs/C$_3$N$_4$. (b) Photocatalytic H$_2$ evolution activities over C$_3$N$_4$, C$_3$N$_4$–NH$_3$, Pt SAs/C$_3$N$_4$, and Pt NPs/C$_3$N$_4$.[44] (c) Schematic of the Pt$_{CL}$-HCNNS and Pt$_{SA}$-HCNNS fabrication.[45]

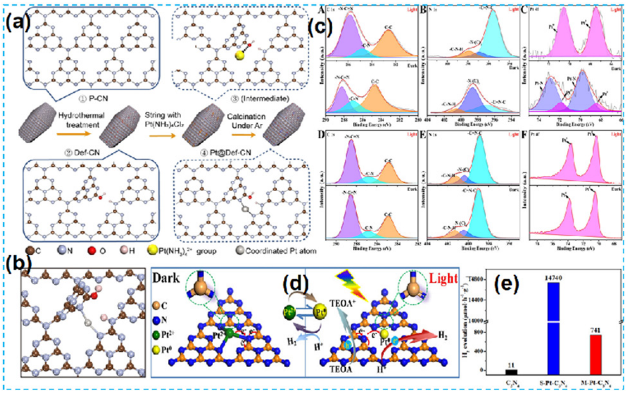

Fig. 7 (a) Schematic illustration for the synthesis of the Pt@Def-CN. (b) The local atomic structure around Pt.[46] (c) SI-XPS high-resolution. (d) Illustration of charge transfer and bond variation on S–Pt–CN catalysts for photocatalytic hydrogen evolution. (e) Comparative presentation of the hydrogen-evolution rates.[47]

3.1.1 Pt. Platinum-based materials are the most effective catalysts for hydrogen evolution. Compared with CN, Pt has a lower Fermi energy level, which is conducive to trapping electrons and thus achieving effective separation of electron–hole pairs.[42,43] Wu *et al.* precisely controlled the anchoring of a single Pt atom. The Pt–N bond formed became a bridge for electron transfer, facilitating the separation of photogenerated carriers (Fig. 6a and b).[44] Duan *et al.* used micro-wet impregnation to similarly form Pt–N bonds to solve the photogenerated carrier recombination problem (Fig. 6c).[45] Of course, the introduction of metal single atoms poses a challenge to adjusting the local coordination environment of the single atoms. In 2022, Xiong's group calcined hydrothermally treated defective CN materials with Pt sources at high temperatures, which allowed Pt atoms to be distributed as single atoms on CN carriers (Fig. 7a).[46] Various characterization effectively demonstrates the coordination environment of Pt atoms. Pt atoms are coordinated with two N atoms of CN (Fig. 7b). The altered coordination environment favours the absorption of electrons by Pt species by promoting hydrogen production. Many studies have explored the chemical bonds exhibited by single-atom catalysts in catalytic reactions with their oxidation states. Still, the mechanism of the dynamic evolution process of single atoms in catalysis is not precise. Bi *et al.* prepared CN-based materials using a simple photochemical synthesis method to observe this dynamic change and further understand the catalytic mechanism.[47] Combining SIXPS (Fig. 7c) with SI-DRIFTS demonstrated the dynamic electron transfer and bonding changes of single-atom Pt and CN under light illumination for the first time (Fig. 7d and e). This work provides excellent insight into the preparation of efficient single-atom catalysts.

Many researchers have inserted Pt single atoms between CN layers to promote the catalytic activity of photocatalysts through interlayer confinement. For example, Xiao *et al.* prepared the interlayer-constrained Pt single atom catalyst using an ion exchange method (Fig. 8a–e). The interlayer constraint can prevent the diffusion of oxygen, thus making the photocatalyst have an excellent antioxidant performance.[48] Zhang *et al.* used the sub-nanometer level of interlayer space to confine single-atom Pt and obtained a relatively high loading (Fig. 8f). In addition to this, considering that the metal atoms inside the nanoparticles hardly participate in the surface reaction leading to the waste of atoms,[49] Ma *et al.* converted Pt nanoparticles to Pt single atoms at high temperatures to enhance the kinetics of the response and reduce the carrier migration resistance (Fig. 8g).[50] It provides an effective method for synthesizing single-atom doping and fundamental insights into the photocatalytic interfacial processes.

3.1.2 Pd. A Pd single atom can also be used as the active site of the hydrogen evolution reaction to improve the catalytic activity of the catalyst. Chen *et al.* inserted Pd single atoms between layers of CN using a simple impregnation and photoreduction method while anchoring Pd to the surface (Fig. 9a).[51] The synthesized sample constructed a channel to facilitate charge transfer, and the surface-anchored atoms were also able to act as active sites to promote hydrogen production (Fig. 9b). Yang *et al.* demonstrated a powerful atomically dispersed Pd co-catalyst by copolymerizing urea-derived supramolecular polymers with NH_4Cl and then wet dipping.[52] Several coordination modes of Pd were constructed in the model, and the adsorption energy of different anchoring sites was calculated by DFT (Fig. 9c). The coordination environment of Pd–N_2 was proved by FT-EXAFS (Fig. 9d). Finally, it is used for efficient photocatalytic H_2 production in water (Fig. 9e). Hou *et al.* introduced synergistic Pd single atoms (PdSAs) and carbon-loaded Pd nanoparticles (NPs) at the interlayer and surface of layered PCNS, respectively. A channel is formed between the Pd single atom and CN to promote electron migration (Fig. 9f), and its optimal hydrogen production reaches 80 micromoles within three hours (Fig. 9g).[53]

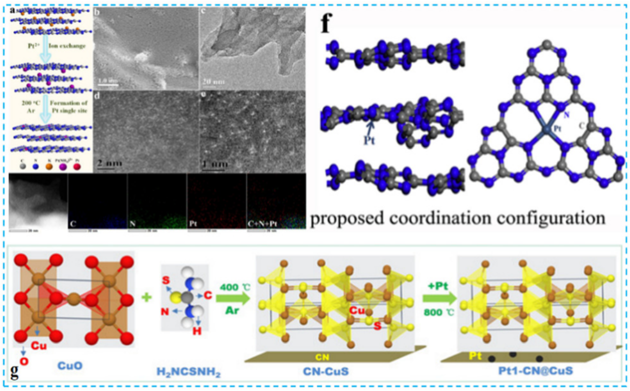

Fig. 8 (a) Illustration of the synthetic procedure of the PtSA/CN photocatalyst, (b) SEM, (c) HRTEM (d) and (e) HAADF-STEM images and the corresponding energy dispersive X-ray (EDX) mappings of PtSA/CN.[48] (f) Illustration of the proposed coordination structure of a confined Pt single atom.[49] (g) Illustration of the preparation of Pt_1-CN@CuS spherical aberration correction.[50]

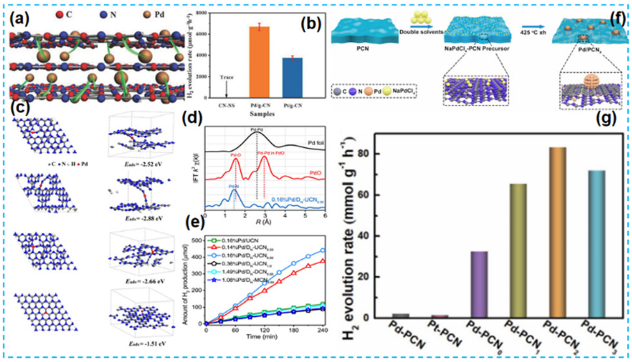

Fig. 9 (a) Conceptual illustration of a Pd/g-CN hybrid with the interlayer intercalation and surface anchor of Pd atom. (b) Photocatalytic H_2 evolution activities of CN-NS, Pd/g-CN, and Pt/g-CN.[51] (c) Possible coordination approaches of Pd SAs with DNUCN and the corresponding adsorption energy of Pd SAs at different anchoring sites. (d) *R* space of 0.16%Pd/DN-UCN$_{0.50}$. (e) Photocatalytic H_2 evolution activity of Pd/CN heterojunctions obtained by different CN nanosheets.[52] (f) Synthesis and structural characterization of Pd/PCNx catalysts. (g) Comparison of H_2 evolution rate for these as-prepared samples under simulated sunlight.[53]

Pd-SACs have been widely used in the catalytic hydrogenation of hydrocarbons and photocatalytic hydrogenation of NO.[54,55] Wang *et al.* introduced a carbon vacancy into CN through heat treatment, and the excess N atoms could form a chemical bond with Pd (Pd–N_3), thus regulating the distribution of Pd in the system (Fig. 10a). The obtained photocatalyst has high and stable photocatalytic activity in the process of NO conversion (Fig. 10b).[56] Yu *et al.* performed DFT theoretical calculations on the synthesized Pd single-atom catalysts (Fig. 10c) to investigate the strong interaction between a single Pd atom and the surrounding N atoms.[57] Both the introduction of carbon vacancies and DFT calculations (Fig. 10d) successfully demonstrated that Pd is anchored to CN and improves the selectivity and stability of nitrogen dioxide (Fig. 10e).

3.1.3 Ag. Ag has been reported to have excellent hydrogen evolution properties. Chen *et al.* doped Ag single atoms into the CN framework in a unique coordination structure to obtain photocatalysts with high loading and catalytic activity. The Ag single atoms were uniformly distributed on CN through a hydrogen bonding self-assembly strategy (Fig. 11a). Hydrogen bond self-assembly is the use of hydrogen bond interaction to assemble molecular subunits of long ordered supramolecular assembly. EXAFS (Fig. 11b and c) showed that Ag was oxidized and could coordinate with CN mutually.[58] The interaction between these two promotes the separation of photogenerated carriers and reduces the hydrogen evolution overpotential, resulting in excellent photocatalytic performance. Single-atom catalysts have more atom utilization, and Yang's paper on single-atom metal nanoparticles describes the entire process of transition from nanoparticles to single atoms.[59] At the same

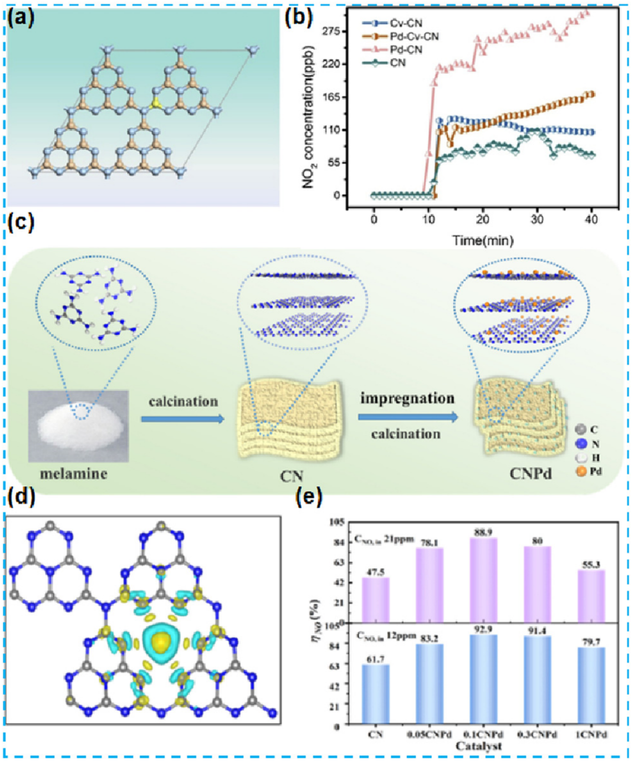

Fig. 10 (a) Schematic model of Pd-Cv-CN: Pd (yellow), N (blue), and C (orange). (b) NO_2 generation.[56] (c) Synthesis and structural characterization of CN, 0.1CNPd and 0.3CNPd. (d) The charge density distribution differences between CN and CNPd. (e) ηNO.[57]

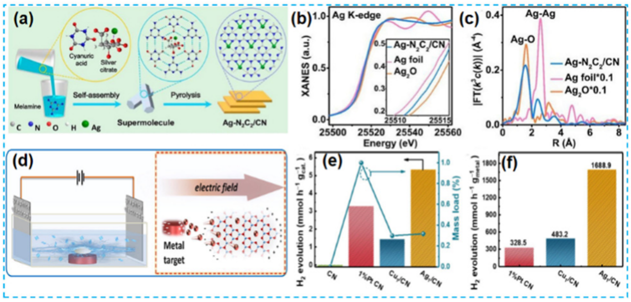

Fig. 11 (a) Schematic illustration of the preparation of $Ag{-}N_2C_2/CN$. (b) Ag K-edge XANES. (c) Fourier transform of Ag K-edge EXAFS spectra.[58] (d) Schematic diagram of the electric-field-assisted fabrication process for SACs. (e) H_2 production rates of the as-prepared samples and mass loadings of isolated metal atoms. (f) H_2 production rates calculated based on the isolated metal atom mass loadings.[60]

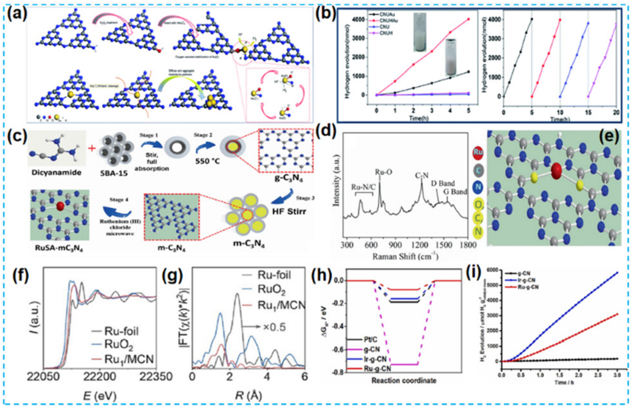

Fig. 12 (a) Schematic of the structural evolution of CNUHAu. (b) Photocatalytic hydrogen evolution activity over CNUAu and CNUHAu under visible light irradiation.[61] (c) Schematic representation of the synthesis protocol for ruthenium single atom over mesoporous C_3N_4. (d) Raman spectra of RuSA-mC_3N_4. (e) Schematic illustration of the Ru coordination with nitrogen in the CN matrix of the RuSA-mC_3N_4 photocatalyst.[62] (f) Ru K-edge XANES spectrum. (g) FT-EXAFS spectrum.[63] (h) The Gibbs free-energy diagram towards the HER of the pristine g-CN, Ir-g-CN, and Ru-g-CN catalysts. (i) Photocatalytic H_2 evolution tests of pristine g-CN, Ir-g-CN and Ru-g-CN catalysts.[64]

time, they explored an electrochemical method to synthesize Ag single-atom photocatalysts (Fig. 11d) and use them for photocatalytic hydrogen production. The hydrogen production is even more effective than the previous work, reaching millimolar orders of magnitude (Fig. 11e and f).[60]

3.1.4 Other noble metal atoms. In addition to Pt and Pd, which are widely used in photocatalysis, other noble metal-loaded photocatalysts have been gradually developed by researchers. For Au, it was found that Au ions alone are quickly reduced to Au atoms and aggregated into nanoparticles on the surface. To solve this problem, Xue *et al.* fixed the single-atom Au by forming stable Au–O coordination (Fig. 12a). This effect effectively inhibits its diffusion to Au nanoparticles, facilitating photocatalytic hydrogen production (Fig. 12b).[61] For Ru, considering the tendency of metal atoms to aggregate into clusters/nanoparticles during preparation, Radek Zbořil *et al.* synthesized RuSA-mC_3N_4 using ruthenium salts, dicyandiamide as precursors and a single atom Ru doped into the CN network structure using a microwave method (Fig. 12c). Raman spectroscopic characterization confirmed the binding of Ru with N/C atoms (Fig. 12d and e). The formed bridge facilitates electron transfer and enhances CO_2 reduction activity.[62] Chen *et al.* stirred the prepared CN material with ruthenium salt, added sodium borohydride reducing agent, and finally obtained powder samples through extraction and washing. The Fourier transform EXAFS spectrum shows that the peak at 1.5 Å is the Ru–N coordination peak (Fig. 12f and g).[63] Liu *et al.* synthesized single-atom Ir and Ru-loaded CN-based photocatalysts using a simple hydrothermal method, respectively. The DFT theoretical calculations reveal that the hydrogen adsorption Gibbs free energy decreases after Ir and Ru loading as a way to promote hydrogen production activity (Fig. 12h and i).[64]

Considering the preparation and application of CN materials doped with noble metals, it is more used in photocatalytic hydrogen production (especially Pd and Pt-based photocatalysts). Its electron configuration is more likely to adsorb protons, improving the hydrogen production performance. The size of some noble metal nanoparticles is reduced to the size of a single atom, which is more efficient for metal atoms. This strategy is beneficial for anchoring the noble metal atoms on CN, effectively inhibiting photogenerated carrier recombination, and shows excellent photocatalytic activity.

3.2 Non-noble metal doping

A great deal of work has been done on CN-based photocatalysts doped with noble metals because of their superior performance. However, they are expensive and scarce. Conversely, the inexpensive incorporation of the remaining transition metals (iron, nickel, cobalt, *etc.*) can also introduce more active sites for redox reactions.

3.2.1 Fe. Among many single-atomic catalysts, atomically dispersed iron catalysts have attracted much attention in the activation process of hydrogen peroxide. This is because the catalytic process fully uses iron and forms an iron reaction center with a high density of electrons.[65] Chemical bonding of iron single atoms with N atoms on CN is expected to activate hydrogen peroxide and degrade antibiotics and pollutants. In 2018, Guo *et al.* selected organic ligand–imidazole coordination compounds (Fe-ICC) as iron sources and prepared catalysts with ultra-small clusters and single-atomic iron sites by one-step pyrolysis of Fe-ICC and melamine (MA) mixtures (Fig. 13a). The N 1s results of XPS showed increased pyridine N content, which was more favorable for binding with Fe atoms (Fig. 13b). Fe species, as the active center, can quickly activate hydrogen peroxide to produce a hydroxyl radical and have a reasonable removal rate of various organic compounds (Fig. 13c).[66] Currently, the mechanism of Fe-modified photocatalytic materials in the catalytic process is not clear, which is the role of single atom Fe or photogenerated electrons and holes. Ren *et al.* further pyrolyzed ferrocene dicarboxylic acid and melamine precursor and synthesized the ideal powder sample after solvent heat treatment. Synchrotron radiation data demonstrate the coordination of Fe–N_4 (Fig. 14a). The iron in the catalyst synthesized by the above method is used as the active site to adsorb the terminal oxygen of persulfate (PMS), which is conducive to the efficient synthesis of monofilament oxygen and the highly selective degradation of wastewater pollutants (Fig. 14b).[67] Wang *et al.* formed Fe–N_4 ligand from the iron porphyrin compound heme (Fig. 14c). The resulting Fe–N_4 site is more favorable to the electron distribution of CN. Adding H_2O_2 as a hole scavenger can be used to promote the separation of photogenerated carriers. Fe single atomic sites promote ROS production through bridging photocatalysis and heterogeneous Fenton reactions.[68] Besides applying Fe-based photocatalysts in degradation, it has specific exploration significance in photocatalytic activation of the C–H bond. In 2022, Fu *et al.* used iron phthalocyanine, an aromatic compound (structure consisting of four pyrrole nuclei), to obtain SA-Fe-TCN by physical stirring and heat treatment. A series of characterization studies determined the coordination environment of Fe–N_4 (Fig. 14d). This electronic structure is conducive to electron transfer, and O_2 molecules are easily converted into O_2^-. Using its high oxidation capacity, the reaction of ethylbenzene to form acetophenone can be enhanced (Fig. 14e).[69]

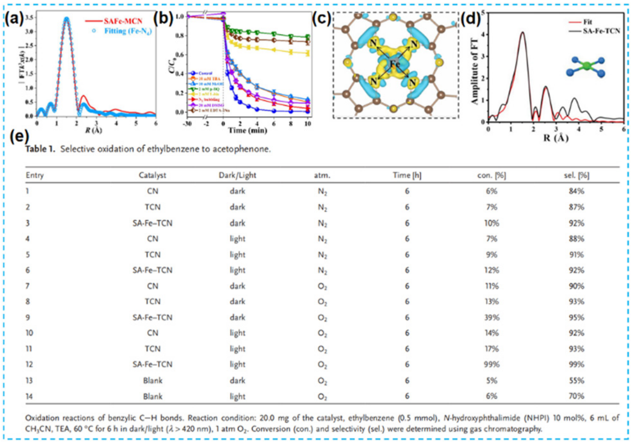

Table 1. Selective oxidation of ethylbenzene to acetophenone.

Entry	Catalyst	Dark/Light	atm.	Time [h]	con. [%]	sel. [%]
1	CN	dark	N_2	6	6%	84%
2	TCN	dark	N_2	6	7%	87%
3	SA-Fe–TCN	dark	N_2	6	10%	92%
4	CN	light	N_2	6	7%	88%
5	TCN	light	N_2	6	9%	91%
6	SA-Fe–TCN	light	N_2	6	12%	92%
7	CN	dark	O_2	6	11%	90%
8	TCN	dark	O_2	6	13%	93%
9	SA-Fe–TCN	dark	O_2	6	39%	95%
10	CN	light	O_2	6	14%	92%
11	TCN	light	O_2	6	17%	93%
12	SA-Fe–TCN	light	O_2	6	99%	99%
13	Blank	dark	O_2	6	5%	55%
14	Blank	light	O_2	6	6%	70%

Oxidation reactions of benzylic C–H bonds. Reaction condition: 20.0 mg of the catalyst, ethylbenzene (0.5 mmol), *N*-hydroxyphthalimide (NHPI) 10 mol%, 6 mL of CH_3CN, TEA, 60 °C for 6 h in dark/light ($\lambda > 420$ nm), 1 atm O_2. Conversion (con.) and selectivity (sel.) were determined using gas chromatography.

Fig. 14 (a) The corresponding EXAFS *R* space fitting curve of the SAFe-MCN. (b) The degradation curves.[67] (c) Bader charge and differential charge distribution.[68] (d) Experimental (black) and fitted (red) EXAFS spectra of the sample with the corresponding structure model. (e) Selective oxidation of ethylbenzene to acetophenone.[69]

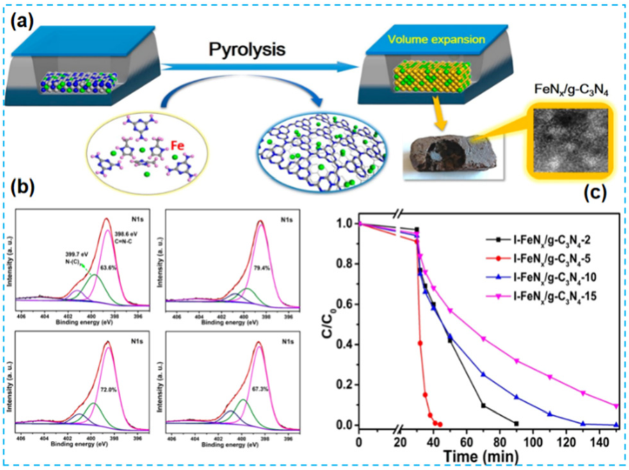

Fig. 13 (a) Pyrolytic synthesis of $FeN_x/g\text{-}C_3N_4$ catalysts. (b) N 1s XPS spectra. (c) Removal efficiency of MB using I-$FeN_x/g\text{-}C_3N_4$-*X* catalysts.[66]

In addition to using organometallic ligands as single atomic metal sources, Tong *et al.* prepared Fe-deposited CN-based materials by mixing iron nitrate inorganic salts with supramolecular gel-assisted thermal polymerization.[70] XPS results showed some interaction of Fe, mainly with N–H groups (Fig. 15a). Finally, the DCF is effectively removed (Fig. 15b).[70] Zhan *et al.* used $FeCl_3$ as a Fe source and modulated Fe single atomic sites by constructing abundant nitrogen vacancies (Fig. 15c). Atomic sites by making large nitrogen vacancies (Fe–N_4) (Fig. 15d). The nitrogen vacancies induced the directional transfer of photogenerated electrons to Fe single-atom sites and stored them, significantly improving the conversion efficiency of H_2O_2 (Fig. 15e).[71]

Based on a summary of the work of Fe-doped CN-based materials, it is found that Fe single atoms are doped into CN in the form of Fe–N_4 coordination. Modified materials are widely used in the photocatalytic H_2O_2 production and the degradation of organic pollutants or antibiotics.

3.2.2 Ni. It has been reported that the d electron of the transition metal single atomic co-catalyst is an effective strategy to enhance photocatalytic performance. Zhao *et al.* changed the electronic structure by introducing the coordination between

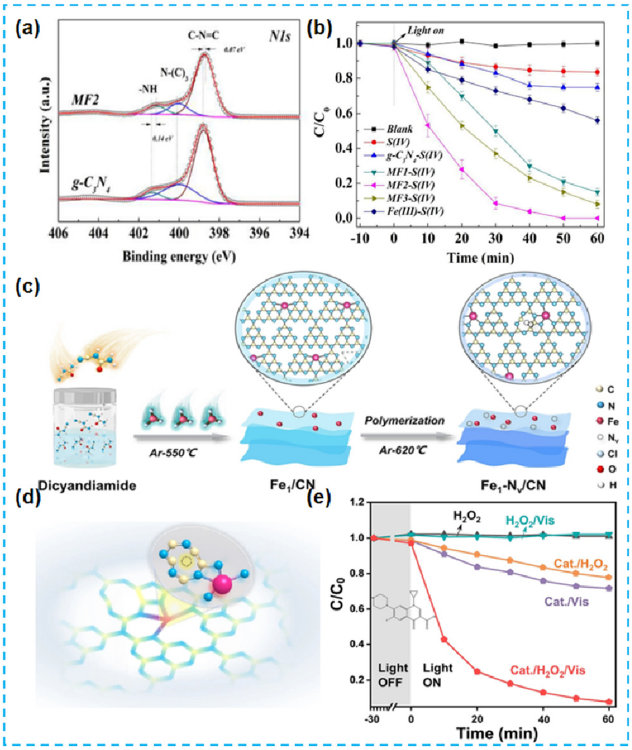

Fig. 15 (a) High resolution XPS spectra of g-C_3N_4 images of MF2 (Fe deposited g-C_3N_4). (b) DCF degradation by different systems.[70] (c) Synthesis of $Fe_1–N_v$/CN ultrathin nanosheets. (d) Schematic model of $Fe_1–N_v$/CN. (e) Degradation curves of CIP in a solely photocatalytic process, Fenton reaction, and photocatalytic activation H_2O_2 process with or without $Fe_1–N_v$/CN.[71]

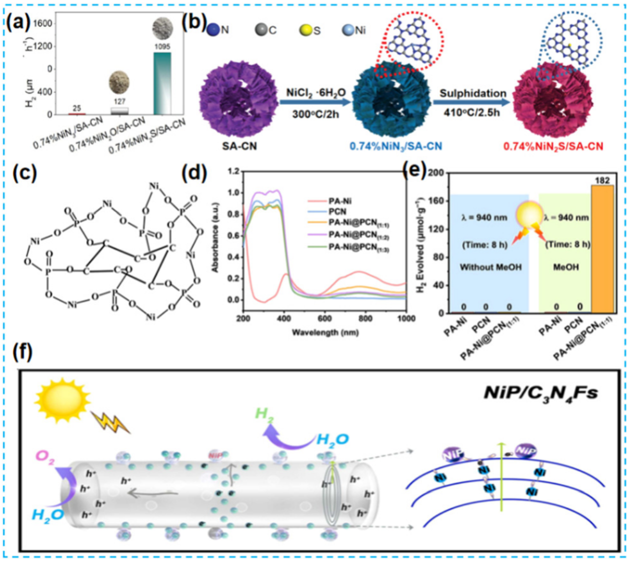

Fig. 16 (a) H_2 evolution rate of 0.74%NiN_3/SA-CN, 0.74%NiN_2O/SA-CN, and 0.74%NiN_2S/SA-CN without Pt as the co-catalyst. (b) Illustration of the synthetic process of 0.74%NiN_2S/SA-CN.[72] (c) Plausible PA-Ni complex structure. (d) UV/Vis-NIR absorption spectra of the as-obtained samples. (e) H_2 evolution amount of the as-prepared sample for 8 h using MeOH conditions and without sacrificial agents.[73] (f) The schematic diagram for electron transfer of the photocatalytic reaction mechanism.[74]

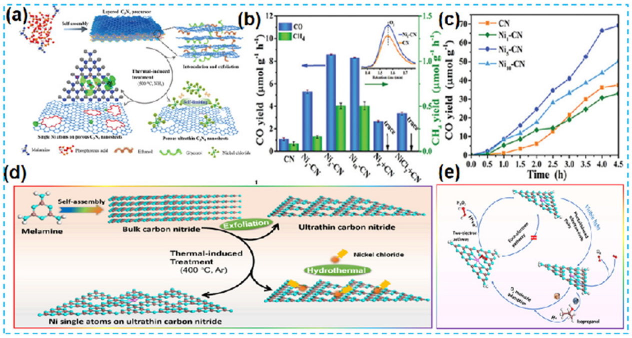

Fig. 17 (a) Schematic illustration for the synthesis of Ni$_5$-CN. (b) Photocatalytic products of CO_2 reduction over Ni$_5$-CN under visible light illumination for 1 h, in comparison with CN, Ni$_1$-CN, Ni$_{10}$-CN, and CN with nickel powders, and CN with $NiCl_2$ (c) The reaction proceeds upon illumination for 4.5 h.[75] (d) Schematic illumination for the fabrication of the NiCN-4 catalyst. (e) Schematic demonstration of photocatalytic H_2O_2 generation for the NiCN-4 catalyst under visible light irradiation.[77]

heteroatoms such as S and single atom Ni and further activating the d electron of single atom Ni to promote photocatalytic hydrogen production (Fig. 16a). They used a two-step heat treatment to obtain a unique electronic structure of Ni coordinated with N and S (Fig. 16b).[72] Shi *et al.* used nickel phytate as a Ni source (Fig. 16c), which is effective as a metal complexing agent to improve the stability of the metal–organic framework. In the mixture of PA-Ni and CN, the PA-Ni species acted as a co-catalyst in the photocatalytic system, which broaden the light absorption range from the visible light to infrared region to enhance the HER (Fig. 16d and e).[73] Song *et al.* chose nickel acetate organic compounds to assemble Ni on the CN surface through solvent heat and pyrolysis. The Ni–N bridge for photogenerated charge transfer was discovered by a series of characterization and other means, which solved the kinetic trouble of charge transport (Fig. 16f).[74] Xiang's group applied a bottom-up synthesis approach (Fig. 17a). CN has a rich porous structure and acts as a vacant ligand to capture monoatomic sites of Ni. The material has Ni in the single-atom cationic electronic state, which provides a clear advantage for electron transfer, thus exhibiting excellent photocatalytic CO_2 reduction activity (Fig. 17b and c).[75] Ni-based single atoms can also enhance H_2O_2 production through a highly selective two-electron oxygen reduction process pathway.[76] Lin *et al.* prepared ultra-thin Ni single atom modified CN materials (Fig. 17d). The DFT theoretical calculation and EXAFS proved the coordination of Ni–N_4. The presence of Ni single atomic sites is conducive to electron accumulation and thus conducive to the photocatalytic generation of H_2O_2 (Fig. 17e).[77]

Of course, as a promising non-noble metal co-catalyst, Ni can be used in photocatalytic hydrogen production and organic reactions.[78,79] Shi's group dispersed $NiCl_2$ in the prepared CN material by freezing deposition so that Ni was evenly distributed on CN. Chemical deposition deposits specific chemicals in solution onto a particular surface. Isolated bright spots with an average size of about 0.2 nm were observed at high angles.

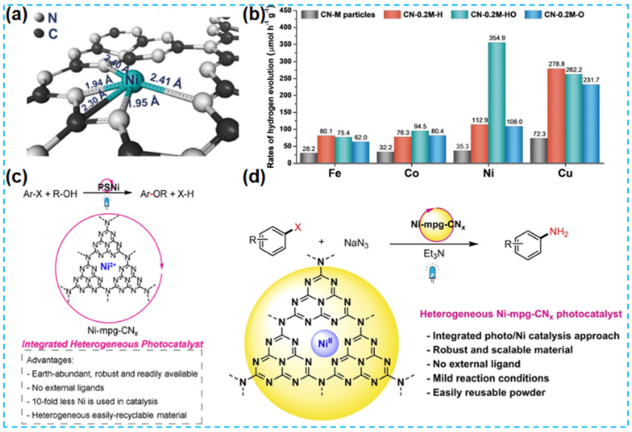

Fig. 18 (a) A schematic model of the Ni single-atom site in CN. (b) Photocatalytic H_2 production rates achieved on either single-atom coordinated CNs or metal nanoparticle-loaded CN. M is the metal species incorporated.[80] (c) The integrated Ni-mpg-CN_x heterogeneous photocatalyst for C–O coupling reported in this study. (d) Methods for primary aniline synthesis.[82,83]

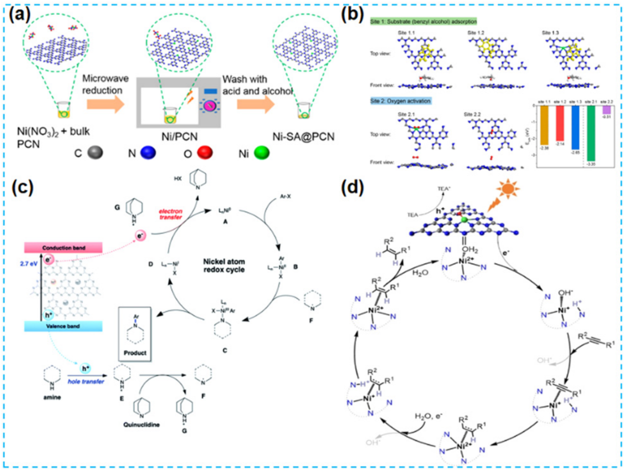

Fig. 19 (a) Diagrammatic illustration of the preparation procedure of Ni-SA@PCN. (b) Theoretical calculations for the absorption of benzyl alcohol (yellow) and the activation of O_2 (red) on PCN based photocatalysts associated with the corresponding absorption energy (ΔE_{ads}) on different binding sites.[84] (c) The proposed mechanism of photoredox C–N coupling on NiSAC/CN.[85] (d) The proposed visible-light-driven semihydrogenation mechanism mediated by single-atom Ni. Here TEA quenched the photogenerated hole on CN, making electrons available for the formation of active Ni^+.[86]

Through Ni K-edge extended X-ray absorption fine structure spectroscopy, it is found that the Ni single atom is only coordinated with C and N atoms. One Ni atom is bonded to four N atoms and one C atom by DFT theory (Fig. 18a). The stability of Ni monoatomic sites in the CN framework is attributed to the coordination's low electronegativity of the N and C atoms. The unique $3d^9$ electron configuration of the Ni monoatomic site makes the CN of the monoatomic coordination easy to excite. The visible light response, charge separation, and transport performance of photocatalysts are improved effectively. Finally, the catalytic activity was evaluated by hydrocracking reaction (Fig. 18b).[80] Kailasam *et al.* dissolved nickel hexahydrate chloride in distilled water and added $NaBH_4$ reducing agent under an inert atmosphere for deposition. The fluorescence intensity of the samples decreased after deposition, indicating improved charge separation. Adding Ni to the catalytic system improved the conversion rate of glycosamines, including aromatic amines. These aromatic amines, in turn, synergistically promoted H_2 production through the PAD strategy.[81] Erwin Reisner synthesized Ni-deposited mesoporous carbon nitride-modified materials by microwave treatment of nickel chloride and mesoporous carbon nitride dispersed in acetonitrile solvent (Fig. 18c and d). The photocatalytic materials synthesized by this method were applied to the C–N coupling reaction and reduction of aromatic azides for two consecutive years. This indicates that microwave-assisted synthesis of photocatalysts has broad applicability.[82,83] The microwave method is widely used for synthesizing catalysts because of its advantages, such as rapid and uniform heating. Lin *et al.* synthesized Ni-SA@PCN. By replacing the conventional heat source with microwave irradiation, the homogeneously mixed sample absorbed microwave energy and reached a high temperature, thus triggering the synthesis of the catalyst (Fig. 19a). The *R*-space of the Ni–N ligand bond length was determined. The Ni single atom was covalently anchored in the PCN structure, promoting the active substrate's uptake and activation (Fig. 19b).[84] Dongwon Yoo *et al.* added the configured aqueous Ni chloride solution dropwise to the suspension of CN in an oil bath. The Ni species was oxidized on CN, which provided versatility for the photo-redox coupling reaction (Fig. 19c).[85] Zhao's group stirred nickel chloride with cyanamide to make it ligate with pyridine N and used the solvent thermal deposition method to obtain monoatomic nickel catalysts. The Ni site is paired with pyridine N of the CN framework, allowing hydrogen to be transported from the most abundant hydrogen source water to the alkyne, resulting in a corresponding alkene with high selectivity (Fig. 19d).[86]

Comprehensive articles on CN materials modified with Ni single atoms are integrated into the CN framework in a Ni–N_4 coordination manner. And such photocatalysts can be applied to photocatalytic organic reactions with some universality. However, the ICP results show that the Ni content mainly fluctuates around 0.5 wt%. Therefore, it provides clues for the subsequent preparation of Ni single-atom modified CN materials.

3.2.3 Cu. Cu single-atom structures have been reported to have good structural stability and catalytic activity, and therefore Cu single-atoms are increasingly being considered for doping into CN framework structures. They use a variety of synthetic methods. Li *et al.* used the simplest two-step method to dope Cu in phosphorus-doped CN by phosphorylation pyrolysis (Fig. 20a), which changed the coordination of Cu from Cu–N_3 to Cu–P_3. The two coordination structures shifted the d-band center of Cu to the Fermi energy level (Fig. 20b) and improved the adsorption of CO_2.[87] Wang *et al.* prepared Cu-*X*/CN by thermal condensation treatment of the precursor only.

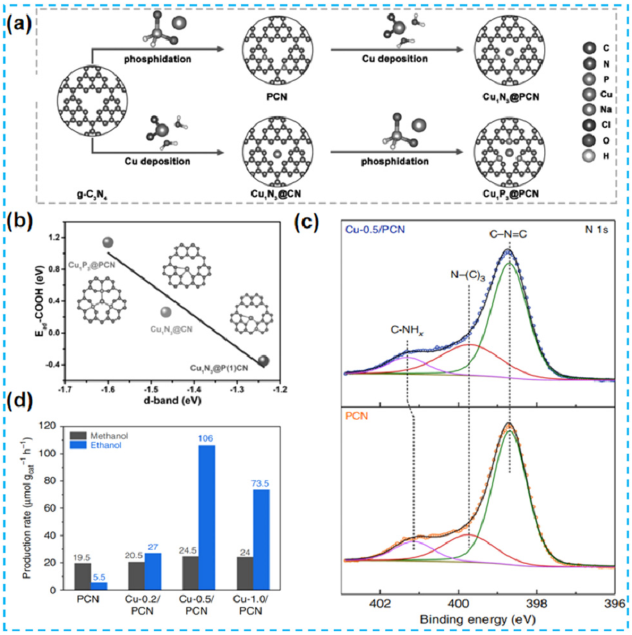

Fig. 20 (a) Scheme of the synthesis of Cu_1N_3@PCN and Cu_1P_3@PCN. (b) The relationship between the d band center and adsorption energy of COOH* on single Cu sites of three model catalysts.[87] (c) N 1s XPS spectra of PCN and Cu-0.5/PCN. (d) Liquid products of methane conversion over PCN and Cu-*X*/PCN.[88]

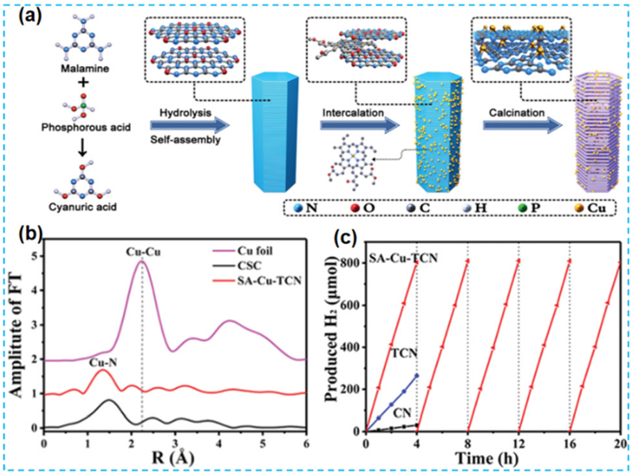

Fig. 21 (a) Schematic illustration of the preparation of SA-Cu-TCN. (b) Fourier transform (FT) of the k^2-weighted Cu K-edge EXAFS (phase shift not corrected) of SA-Cu-TCN, CSC, CuO, and Cu foil. (c) Temporal H_2 evolution under visible light irradiation (λ > 420 nm).[89]

XPS detected the morphology of Cu (Fig. 20c), which forms complexes with CN: Cu is coordinated to sp^2-hybridized N atoms. The presence of Cu sites promotes methane adsorption and activation (Fig. 20d).[88]

In recent years, the self-assembly technology of nanomaterials has been widely used in optoelectronics, biopharmaceuticals, and chemicals. After self-assembly, the final structure has the lowest free energy. Fu's group first prepared the supramolecular precursors from melamine and subjected them to *in situ* hydrolysis and self-assembly in phosphoric acid. Cu single atoms were inserted between the layers (Fig. 21a). The doping of Cu promoted the exfoliation of CN, which led to an increase in the specific surface area of the material. EXAFS revealed the presence of Cu–N bonds (Fig. 21b). DFT theoretical calculations were performed to confirm the coordination environment: Cu atoms were coordinated to amino and pyridine N. The photogenerated electrons are transferred between the Cu single atom and the N atom of the CN. The new charge transfer channel improves the charge mobility and has a higher rate of photocatalytic hydrogen production (Fig. 21c).[89]

Similarly, Zhao *et al.* first prepared supramolecular precursors (Fig. 22a). But in this work, the Cu source was introduced, and the Cu-containing supramolecular precursors were directly prepared with subsequent heat treatment. To investigate the local coordination structure, the wavelet transform of FT-EXAFS identified that there was no Cu–Cu coordination; XPS data showed the presence of both Cu–O coordination and Cu–N coordination (Fig. 22b). For both coordination structures of Cu, the O atom has a stronger electrophilicity than the N atom. Hence, the Cu_1–N_1O_2 site is more favourable for charge distribution (Fig. 22c), making the electron transfer between the CN substrate and the Cu active species more efficient.[90] Many studies have anchored single atoms to the CN surface. Xu *et al.* placed Cu in the CN bulk phase to investigate its role. This work developed a simple liquid-phase preorganization method to synthesize Cu-containing CN-based materials (with chemical bonding between Cu and pyridine N) (Fig. 22d). The results of the power function measurements show an increase in the Fermi energy level of the samples, further demonstrating the substantial electronic effect of the Cu metal species. Modifying single atoms with the metal electronic structure's

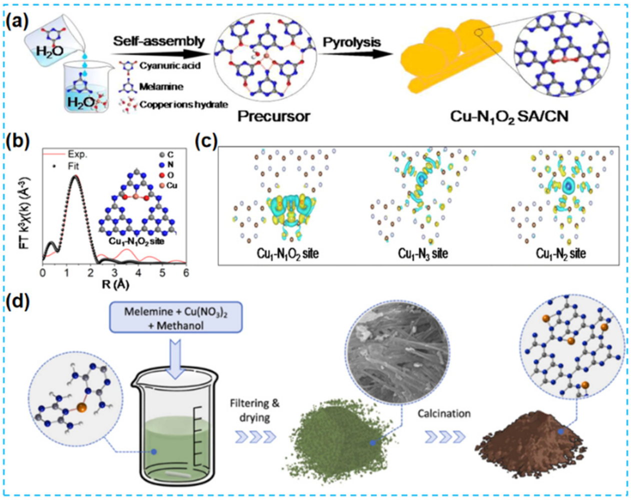

Fig. 22 (a) Schematic illustration of the preparation of SA-Cu-TCN. (b) EXAFS fitting curve in *R* space and the model of the Cu_1–N_1O_2 site. (c) Differential charge density of Cu_1–N_2, Cu_1–N_3, and Cu_1–N_1O_2 coordination configuration.[90] (d) Schematic illustration of the preparation process of CN-xCu samples.[91]

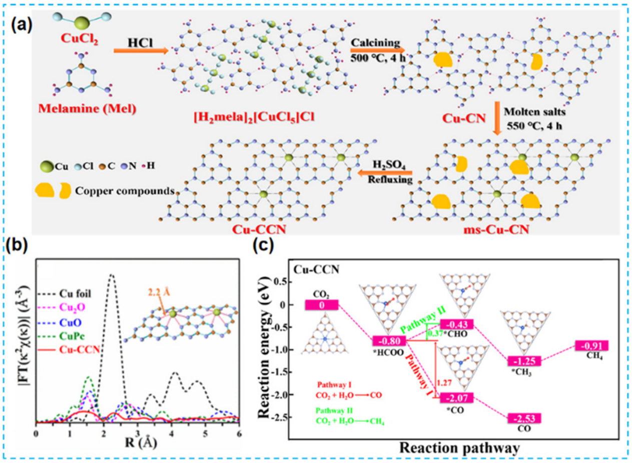

Fig. 23 (a) Schematic diagram of the synthesis process over Cu-CCN samples by using the melamine and $CuCl_2$ as a pre structure of the as-prepared samples. (b) The model of the introduction of a single Cu atom into carbon nitride. (c) Reaction pathways for photocatalytic CO_2 reduction and the corresponding chemical molecular structure on Cu-CCN samples based on DFT calculation.[92]

design promotes the materials' photocatalytic activity in cross-coupling reactions.[91]

Amorphous CN materials have many defects compared to the crystalline state, and introducing single atoms on top of this will limit photocatalytic activity. Therefore, Xiang's group considered this problem and used molten salt and reflow methods to prepare crystalline CN-based materials capable of anchoring Cu single atoms (Fig. 23a). The Cu sites (Fig. 23b) can be used as active centers for CO_2 adsorption and thus have high selectivity and energy conversion for CO_2 (Fig. 23c).[92]

In recent years, it has been found that in addition to the introduction of a single atom, heteroatom coordination is introduced into the system. This strategy can effectively adjust the electron configuration. Cu-Modified CN-based photocatalysts are widely used in various fields of photocatalysis.

3.2.4 Other non-noble metal atoms. In addition to the commonly used non-noble metals, the rest of the transition metals were loaded on CN as well. Shen *et al.* used an intermediate coordination strategy (Fig. 24a), $ZnCO_3$, to provide Zn atoms for synthesizing the Zn–PCN. With the increase of Zn loading, the specific surface area of the catalyst gradually increased, enriching the active site of the reaction. Electrons are transferred from the Zn atoms to the carbon nitride. EXAFS showed that the N coordination of hexavalent pyridine (Zn–N_6) is the predominant coordination structure in Zn–PCN (Fig. 24b).[93] Zhou *et al.* formed Zn–N_3 coordination structures by simple pyrolysis of Zn single atoms inserted into CN (Fig. 24c), enhancing visible light absorption and separating electron–hole pairs (Fig. 24d).[94] To find a photocatalyst with dual functional, active sites for hydrogen and oxygen precipitation, Yao *et al.* designed a two-component synergistic photocatalyst containing Co SAs and PtCo alloys loaded on nanosheet CN. Combined with theoretical calculations, the Co monoatomic sites acted as active sites for hydrogen precipitation. At the same time, the PtCo alloy could work as an active site for oxygen precipitation, which resulted in a catalyst with high atomic utilization and activity (Fig. 24e).[95] The synthesis of Mo-doped CN materials using a condensation method by Zhou *et al.* resulted in the phase transition of CN from crystalline to amorphous and the formation of new chemical bonds (Mo–N, Mo–C) (Fig. 24f). The CN-based materials synthesized by this method effectively facilitated the separation of photogenerated carriers.[96] In addition, the radius of Nb is reported to be smaller than the triazine ring radius of CN, while the unique d orbital of Nb ($4d^45s^1$) also provides many impurity bands for CN. When single-atom Nb is anchored on the surface of CN, it can easily replace N vacancies and form coordination with C atoms. Therefore, Wang *et al.* loaded single-atom Nb on N-defect-rich CN materials. The formed Nb–C bond promotes charge transfer (Fig. 24g): Nb acts as an electron-absorbing site and promotes the migration of photogenerated electrons around Nb, effectively separating the carriers. Thereby enabling CO_2 reduction capabilities.[97]

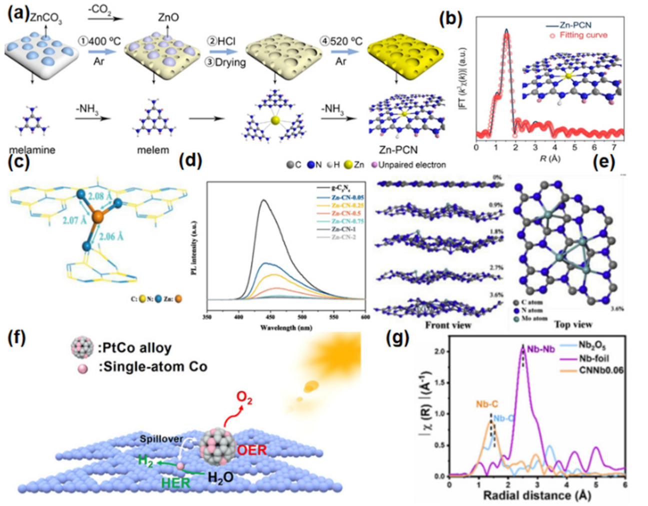

Fig. 24 (a) Schematic illustration of the synthesis of Zn–PCN. (b) The structure model of Zn–PCN with one Zn atom coordinated by six N atoms.[93] (c) DFT-calculated Zn-CN structure. (d) PL of single Zn atom doped g-C_3N_4.[94] (e) Catalyst mechanism diagram.[95] (f) The optimized structure of (0–4%) Mo atoms on the g-C_3N_4 surface.[96] (g) FT $k^3(R)$Nb K-edge EXAFS.[97]

4 f region element doping

Furthermore, rare earth single-atom catalysts' loading materials and mechanisms are still poorly studied. Dong *et al.* only used a thermal treatment (Fig. 25a) to synthesize La single-atom catalysts.[98] XPS results (Fig. 25b) showed that the binding energy of the loaded single-atom La decreased, mainly due to a shift toward lower binding energies due to the electronic structure rescaling and relaxation effects. Its use as an active site promoted photocatalytic activity. Tian *et al.* encapsulated rare earth Ce single atoms in CN nanosheets (Fig. 25c), and a series of characterization studies showed the coordination

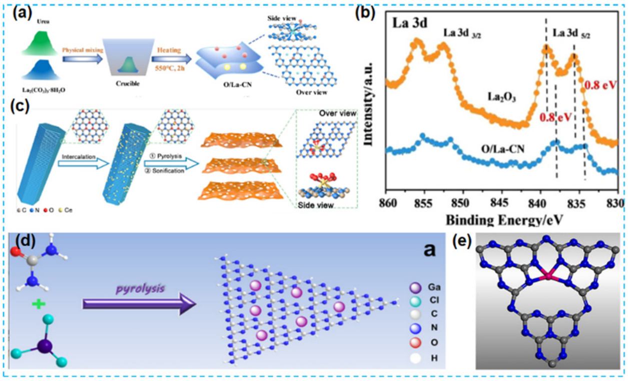

Fig. 25 (a) Schematic diagram of catalyst synthesis processes. (b) XPS spectra.[98] (c) Schematic diagram of the synthetic procedure of the single atom Ce photocatalyst.[99] (d) The schematic diagram of GCN synthesis. (e) The GaN_4 site structure model in GCN.[100]

environment of single atoms in CN: $Ce–N_4/O_6$. The unique coordination structure synergistically regulates the electron's local environment and accelerates the separation of photogenerated carriers. The catalysts loaded by the single atoms exhibit excellent hydrogen production performance.[99]

5 p region element doping

In addition to transition metals, researchers have also paid extensive attention to post-transition metals. It has been reported that Ga atoms can achieve regional enrichment of photogenerated electrons and improve the efficiency of photogenerated carrier separation. Sun *et al.* designed and synthesized novel efficient Ga-doped CN hydrogen photocatalysts using a simple thermal polymerization method (Fig. 25d). The coordination between single Ga atoms and N atoms exists to form $Ga–N_4$ (Fig. 25e).[100] The excited state electrons stored in the GaN_4 sites have longer lifetimes and have more opportunities for proton adsorption and electron transfer. Since the hydrogen adsorption energy on the GaN_4 site in the ground state is positive, it promotes the desorption process after electron transfer to hydrogen. Its photocatalytic hydrogen production performance is 162 times higher compared to bare CN. Al, which is in the same group as Ga, was also designed as a monometallic dispersion by the researchers. Han *et al.* synthesized Al-doped CN materials by freeze-drying treatment followed by thermal polymerization. The Al metal sites were able to modulate the charge density distribution in the valence and conduction bands of CN; electron transfer channels were constructed between adjacent layers of CN to achieve efficient electron transfer.[101]

To sum up, many researchers have reduced the size of metal atoms to the size of single atoms through thermal polymerization, chemical deposition, and other methods to synthesize efficient photocatalysts for modifying CN materials by single-atom doping. Single metal atoms bond with N atoms on CN to construct a charge-transfer bridge and promote photogenerated carrier separation and transfer.

6 Dual-atom doping

Although single-atom catalysts have made some achievements, there are still some challenges. Since single-atom catalysts only have single active centers, the catalytic pathway with multiatom may be inhibited and it is hard to break the linear relationship, which fundamentally limits the catalytic efficiency.[102] Diatomic doping has become a research hotspot because of its abundant active sites and good structure–activity relationship.

6.1 Noble and non-noble metals

Currently, the most reported high-activity catalysts are mainly noble metal-based catalysts. Noble metal-based catalysts can maintain catalytic activity in various environments and have multiple applications. However, due to the high cost of noble metals and their scarcity, many researchers have first replaced one of the metals in the diatomic loading with a non-noble metal. Lu *et al.* synthesized different diatomic CN-based materials by modulating the site-resistance effects of two metal precursors (Fig. 26a), Pt and Ni, to reduce the cost while maintaining the excellent chemical activity of the catalysts. Among them, the photogenerated electrons migrate from Pt to Ni active sites; the bifunctional synergy of PtNi effectively promotes hydrogen production (Fig. 26b).[103] According to literature research, composite catalysts composed of Co and Ru atoms play an exciting role in the investigation of CO_2 reduction. Therefore, Xiang *et al.* integrated CoRu bimetallic atoms into conjugated CN structures. Co acts as a charge transfer mediator, and Ru acts as an adsorption site in the CO_2 reduction process, which enhances the CO_2 reduction activity to a certain extent (Fig. 26c and d).[104] Copper, a non-noble

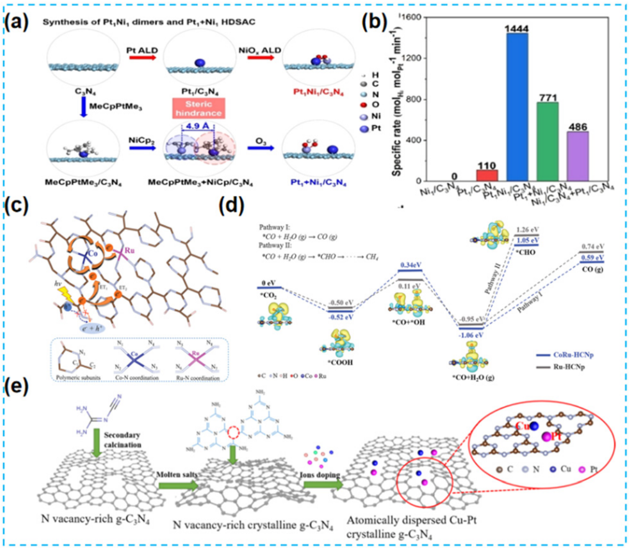

Fig. 26 (a) A schematic illustration of the synthesis of Pt_1Ni_1 oxo dimers and $Pt_1 + Ni_1$ HDSAC. (b) The specific rates of the above samples based on the Pt loadings.[103] (c) Schematic illustration of selective CO_2 adsorption and the proposed dynamic photocarrier transfer mechanism in bimetallic Co–Ru single-atom-doped conjugated carbon nitride polymer. (d) Theoretical photocatalytic deoxygenation mechanism of CO_2 to CO.[104] (e) Schematic illustration of the synthetic procedure for PtCu-crCN.[105]

metal atom, is much more abundant on the earth than noble metals. The introduction of copper into the catalyst can significantly reduce the cost. Xiang *et al.* combined Pt and Cu into the N vacancy-rich CN framework the following year, forming an isolated and stable Pt species with Cu species (Fig. 26e). The presence of the double atoms improved the CO_2 conversion by promoting synergistic interactions and reaction kinetics.[105]

6.2 Non-noble and non-noble metals

Suppose the binary atoms are adjusted to non-noble metal atoms. In that case, the original cost of the synthesis catalyst will be reduced more significantly, which is more in line with the sustainable development of the world economy today.

For Fe-based photocatalysts, researchers have synergized them with metal atoms such as Co, Ni, W, and Mn to enhance the activity of the intrinsic catalysts. Niu *et al.* used soft-molded precursors to synthesize CN catalysts doped with metal Fe and Co single atoms. The resulting two-site effect changed the framework's coordination environment and constructed a transfer "channel" for photogenerated carriers. This leads to the efficient degradation of TBBPA.[106] Inspired by the excellent work, Jiang *et al.* prepared Fe-, Co-, and O-co-doped CN by a simple calcination method. The samples showed an increased specific surface area and enhanced electron transfer capability.[107] Lu *et al.* prepared FeW bimetallic atom-anchored carbon nitride-based photocatalysts by prefixation and pyrolysis. The materials synthesized in this work, Fe and W, respectively, form chemical bonds with N to stabilize in the CN matrix element. DFT calculations showed that the Fe active site had a good adsorption ability to PMS and improved the photocatalytic efficiency.[108] Asefa *et al.* considered introducing a large amount of non-toxic and abundant Fe and Mn elements to enhance the degradation ability of the photocatalyst.[109]

It has been reported that Co-based catalysts (Co single atom, Co diatomic, Co-based heteroatomic) have been developed and have some effectiveness in CO_2 reduction. Li *et al.* synthesized Mn_1Co_1/CN photocatalysts by supramolecular self-assembly (Fig. 27a). Isolated bright spots in HAADF-STEM were identified as Mn and Co atoms (Fig. 27b–e); the loaded Mn and Co can act as redox sites (Mn sites are suitable for trapping holes, and Co sites are good for absorbing CO_2) to promote photogenerated charge transfer (Fig. 27f), thus facilitating CO precipitation.[110] Lin *et al.* used a template-free method for one-pot. The formation of Co–N and Mo–N bonds is favorable for photocatalytic activity (Fig. 27g–i).[111]

For Cu-based catalysts, Cu currently plays a crucial role in enhancing the adsorption of *CO intermediates and promoting the formation of *COCO due to its ability to bind to *CO to support *COCO bond coupling in CO_2 conversion.[112] In 2022, Guo *et al.* prepared a polymeric carbon nitride photocatalyst containing indium–copper bimetal using a simple thermal polymerization method (Fig. 28a). It was shown that the catalyst had good photocatalytic activity, mainly due to the promotion of charge transfer from the carbon nitride to the metal sites in synergy with the bimetal, facilitating charge separation (Fig. 28b).[113] p–d block In-based bimetallic catalysts with atomic dispersion were developed by Guo *et al.* Cu–In catalysts were synthesized using a thermal polymerization method using CuCl as the Cu source (Fig. 28c). The introduction of Cu enhanced the light absorption ability of the catalyst (Fig. 28d); the Cl atom in the structure promoted charge separation and modulated the electronic network of the CuIn sites, ultimately reducing the reaction activation energy (Fig. 28e).[114] Choi *et al.* used a simple physical hybrid thermal copolymerization method to synthesize CN by embedding Sn and Cu in CN frameworks at adjacent positions. CN was demonstrated by *in situ* IR spectroscopic characterization to have intermediates adsorbed on the di-single atom active sites.[115] This strategy is expected to be widely used in photocatalysis.

In summary, it is found that it is necessary to construct dual active sites in CN to promote photocatalytic activity. In contrast to a single atom, a single living species in a diatom can be prevented from coming together by interaction with neighboring atoms. The formation of dual active sites maximizes

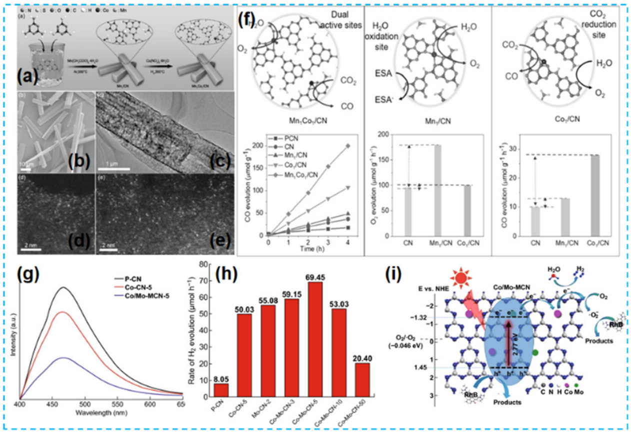

Fig. 27 (a) Synthesis of the Mn_1Co_1/CN catalyst. (b) SEM and (c) TEM images of Mn_1Co_1/CN. AC HAADF-STEM image of (d) Mn_1/CN and (e) Mn_1Co_1/CN. (f) Photocatalytic activities of samples with double single-atom active sites for CO_2 reduction.[110] (g) Photoluminescence spectra of P-CN, Co-CN-5, and Co/Mo-MCN-5. (h) Photocatalytic H_2 evolution rate of the as-prepared materials. (i) Photocatalytic mechanism scheme of Co/Mo-MCN under visible light irradiation.[111]

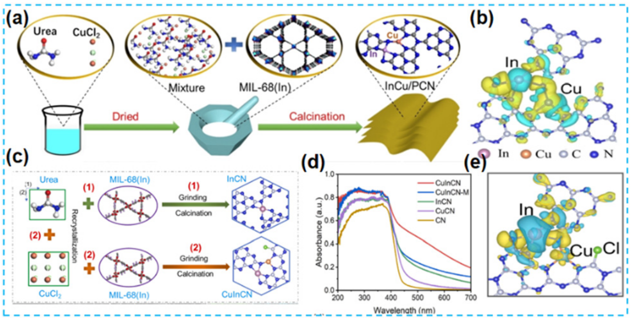

Fig. 28 (a) Illustration of the synthetic process used in producing InCu/PCN. (b) Illustration of the synthetic process used in producing InCu/PCN.[113] (c) Schematic diagram of the prepared process for InCN and CuInCN. (d) UV-Vis absorption spectra. (e) Charge density.[114]

atomic utilization, and the synergistic effect between the two will promote the selectivity of the reaction (mainly when applied to photocatalytic CO_2 reduction).

7 Photocatalytic applications of CN-based materials

An all-in-one photocatalyst was constructed by introducing metal atoms into CN. Metal atoms, as active centers, also act as co-catalysts. This can change the electronic structure and promote the separation of photogenerated carriers, improving H_2, H_2O_2 production and photocatalytic CO_2 reduction. The photocatalytic mechanism of CN-based photocatalysts did not change regardless of the method of doping the metal atoms into the CN framework. The whole process of photocatalysis is mainly divided into the following steps (Fig. 29): (1) the semiconductor photocatalyst receives energy from sunlight; (2) the electrons in the valence band in the semiconductor leap to the conduction band, leaving holes in the valence band and getting electrons in the conduction band; (3) the photogenerated electrons and holes partly recombine in the bulk phase and partly migrate to the semiconductor surface; (4) the photogenerated holes and electrons migrating to the surface still exist partly in the surface, while the remaining photogenerated carriers undergo a series of oxidation (mineralization of organic pollutants) reduction (HER, CO_2 reduction) reactions at the surface.

7.1 Photocatalytic hydrogen production

Hydrogen (H_2) is one of the most promising energy sources. This is well known. It is non-toxic, environmentally friendly, and has a high energy density. Using inexhaustible solar energy as the primary energy source to decompose water is one of the methods to produce clean hydrogen energy. Photocatalytic H_2 production is one of the ideal H_2 production technologies.

The following table (Table 1) summarizes the H_2 production of CN materials modified by metal atom doping over the last five years.

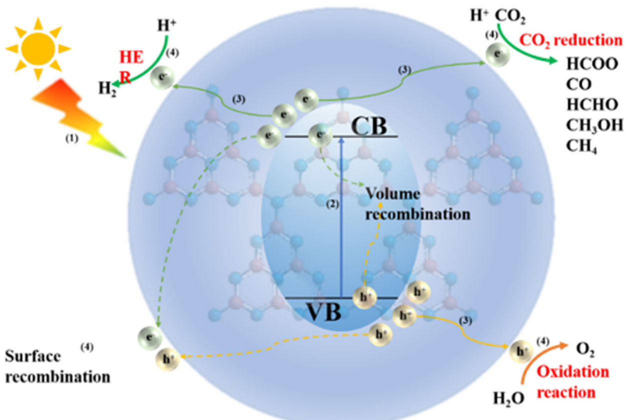

Fig. 29 Photocatalytic mechanism diagram.

7.2 Photocatalytic CO_2 reduction

Currently, the global warming trend is becoming more and more serious. The most direct cause of the greenhouse effect is the increasing emission of CO_2 in the air. According to various reports, the concentration of CO_2 in the atmosphere is too high. Suppose it continues to be emitted in large quantities. In that case, the global temperature will rise, leading to the drying of subtropical areas, an increase in rainfall at high latitudes, the reduction of icy ocean regions, and the early melting of snow and ice. To protect the Earth's ecological environment, on which human beings depend, people have to consider measures to control CO_2. Although CO_2 negatively affects the ecological climate when emitted in large quantities, it is one of the essential resources in nature; therefore, the research into CO_2 resource recovery technology has received much attention in recent years. The photocatalytic CO_2 reduction technology is of great importance in improving the environment.

Semiconductor photocatalysts are excited after absorbing photons of specific energy, and the electrons generated by the excitation will combine with CO_2 molecules to produce CO, HCOOH, HCHO, CH_3OH, and CH_4. It is similar to photocatalytic hydrogen production, and both are reduction reactions (Table 2).

7.3 Photocatalytic production of H_2O_2

Photocatalytic hydrogen production uses the electrons generated by the catalyst to promote the activity, *i.e.*, the reduction reaction. Hydrogen peroxide production uses the holes left in the valence band of the photocatalyst by photoexcitation to act: oxygen in the air will interact with the holes to produce superoxide radicals, which combine with protons (H^+) and then use photogenerated electrons to make hydrogen peroxide. Hydrogen peroxide, an environmentally friendly oxidant, is widely used in pulp bleaching, medical disinfection, and other fields. The conventional method of hydrogen peroxide production is not conducive to the sustainable production of H_2O_2. The catalytic production of H_2O_2 using CN semiconductor photocatalysts is a green and efficient production strategy. Table 3 summarizes the comparison of H_2O_2 production in the last five years (Table 3).

8 Discussion of the intrinsic properties of catalysts

8.1 The stability of catalysts in application

In the current research on the performance of photocatalysts, the stability of photocatalysts is also one of the important indicators of their photocatalytic performance. It has been reported that noble metal catalysts can maintain their catalytic activity stably under various environments. Combining metals with CN carriers by bonding results in an even more efficient and stable material.

In numerous studies, the structural stability of the catalysts was evaluated by various characterization of the catalysts after the reaction. Yin *et al.* also compared the reacted catalysts with

Table 1 Summary of representative photocatalytic H_2 evolution using CN under visible light

Photocatalyst	Metal loading	Light source	HER (μmol h^{-1} g^{-1})	Ref.
Pd/g-CN	0.17 wt%	Xe	6688	51
K-CN	10 wt% KBr	$\lambda > 400$ nm (Xe)	1337.2	33
CN-KI	—	$\lambda > 420$ nm (Xe)	1611	116
NiSCN	5 wt%	$\lambda > 420$ nm (Xe)	2021.3	117
CN-0.2Ni	0.2 at%	Xe	354.9	80
Co/Mo-MCN	Co: 0.081% Mo: 0.058%	$\lambda > 400$ nm (Xe)	694.5	111
CNUHAu	0.18 wt%	Xe	789.1 nmol h^{-1}	61
CoNiSx-CN	Co: 0.739%	$\lambda > 420$ nmLED	2366	118
NCN	20.55 wt%	Xe	155.71	119
CNNC-15	15 wt%	$\lambda > 420$ nm (LED)	2088.28	120
S-Pt-C_3N_4	0.32 wt%	Xe	14 740	47
Ag-N_2C_2/CN	—	$\lambda > 420$ nm (Xe)	1866	58
S + K-g-C_3N_4	K: 9.88% S: 0.065%	$\lambda > 420$ nm (Xe)	8780	121
SA-Pt/C_3N_4	8.7 wt%	$\lambda > 420$ nm (Xe)	22 650	49
SA-Cu-TCN	0.3 wt%	$\lambda > 420$ nm (Xe)	10 600	89
Pt_1-CN@CuS	—	LED-530	25.4 μmol h^{-1}	50
g-CN-X (X = Br or I)	—	$\lambda > 420$ nm (Xe)	5880	122
PANi@PCN	16.23%	AM 1.5G	2560	73
Co-g-C_3N_4	Co: 0.07 wt%	$\lambda > 420$ nm (Xe)	12 300	123
AgSACs	0.31 wt%	$\lambda > 400$ nm (Xe)	5333.3	60
Pd/PCN_2	5.10 wt%	AM 1.5G (Xe)	83 340	53
Zn-PCN	4.79 wt%	$\lambda > 420$ nm (Xe)	1172.9	93
Pd/D_N-UCN	0.16%	320–780 nm	22 080	52
Pt_{SA}/g-C_3N_4	0.6 wt%	Xe	11 600	48
Ru-g-CN	Ru: 0.24 wt%		1175	
Ir-g-CN	Ir: 1.71 wt%	LED	2122	64
Pd-PCN	0.2 wt%	$\lambda > 420$ nm (Xe)	16 591	124
Cu-g-C_3N_4	—	$\lambda > 420$ nm (Xe)	526	125
Au/g-C_3N_4	—	150 W Xe	1061.82	126
1.0%-Pt/CN	1 wt%	$\lambda > 420$ nm (Xe)	2316	127
Ag_1/CN	1 wt%	$\lambda > 400$ nm (Xe)	3690	59
Ni_1-N_2S	0.74 wt%	$\lambda \geq 420$ nm (Xe)	1095	72
MO-PCN	0.92 wt%	AM 1.5G (Xe)	3000	128
(Ni/C_3N_4Fs)	—	$\lambda > 420$ nm (Xe)	1890	74
PtSA-CN620	3.45 wt%	$\lambda > 420$ nm (Xe)	3020	129
Mo-C_3N_4	—	$\lambda > 420$ nm (Xe)	37	96
PtSAs/C_3N_4	—	Xe	11 472	44
CoSAs/PtCo	—	Xe	5580	95
Ce-SA-C_3N_4	0.26 wt%	$\lambda > 420$ nm (Xe)	33 500	99
P-CN(Cu)	—	$\lambda > 420$ nm (Xe)	6530	130

the unreacted catalysts. The XRD spectra and FT-IR spectra of the catalysts before and after the reaction were not significantly different as shown in Fig. 30a and b. ICP analysis showed that a strong chemical bonding force formed between the atoms and the CN carriers resulted in no significant decrease in the atomic content before and after the reaction. The Co content changed from 0.739% to 0.702% and the Ni content changed from 0.126% to 0.118%.[118] Hou *et al.* performed XPS characterization of the catalyst before and after the reaction, and its N 1s energy spectrum showed three similar peaks, indicating that W-PCN600 had high structural stability (Fig. 30d).[128] Tian *et al.* characterized the post-reaction catalyst Ce-SA-C_3N_4 by XRD, FT-IR, and HAADF-STEM (Fig. 30c). After a long time of hydrogen production test, the structure of the sample did not change, and the single atom Ce maintained a good dispersion.[99] Wang *et al.* found no significant change in the XPS-fitted peaks of the reacted Ni 2p.[135] Choi *et al.* compared the XPS spectra of Cu 2p and Sn 3d before and after the reaction. The results showed that the valence states of the metal atoms did not change after the 24 h reaction. The VB position was only slightly reduced and negligible.[141] Guo *et al.* observed the HRTEM of the sample after the reaction and found that Pt nanoparticles were observed in Fig. 30e. However, the catalyst was not deactivated in the hydrogen production test.[129]

Through a series of structural characterization studies of the post-reaction photocatalyst and the initial catalyst, we found that the photocatalyst has good structural stability. However, other studies have found that metal atoms can leach out or fall off during the reaction. Therefore, how to stably attach metal atoms to CN carriers is a critical issue for practical industrial applications.

8.2 Repeatability and sustainability of catalysts

In the test of photocatalytic performance, the repeatability of photocatalysts is generally assessed by the cyclic test. Liu *et al.* investigated the stability of Ir-CN and Ru-CN. The H_2 production of the catalyst can remain constant for at least three cycles (Fig. 31a).[64] Jiang *et al.* tested the stability of Pt/CN-BH-H over four cycles (Fig. 31b).[127] Qi *et al.* also tested the photocatalytic H_2 production of NiSCN5 in four cycles (Fig. 31c).[117] Wang *et al.*

Table 2 Representative summary of photocatalytic CO_2 reduction using CN under visible light

Photocatalyst	CO_2 reduction (μmol h^{-1} g^{-1})	Ref.
Ni_5-CN	CO: 8.6	75
O/La-CN	CO: 92	98
Cu-CCN	CO: 3.086	92
CoRu-HCNp	CO: 3824	104
Mn_1Co_1/CN	CO: 47	110
Pd_1 + NPs/C_3N_4	CH_4: 20.4	131
Pt@Def-CN	CH_4: 6.3	46
Cu-g-C_3N_4	CH_4: 2.4	125
Cu_1N_3@PCN	CO: 49.8	87
P/Cu SAs@CN	C_2H_6: 616.6	132
(FeN_4/K-g-C_3N_4)	CO: 20.00	133
PtCu-crCN	CO: 11.74	105
InCu/PCN	C_2H_5OH: 28.5	113
K/S@CN-0.5	CO: 16.27	134
Mo-C_3N_4	CO: 18	96
RuSA-mC_3N_4	CO: 250	62
Ni/S-CN-N	CO: 5860 CH_4: 1890	135
CN-KRb	1212.3	136
CNNb0.06	CO: 110.6	97
Sn_x-Cu_{100-x}/C_3N_4	HCHO: 10.79	137
IL/Co-bCN	CO: 160	138

evaluated the reusability of Ni/S-CN-N through the cyclic degradation of tetracycline (TC). After the fifth cycle, the removal rate can still reach 83.33% (Fig. 31d).[135] Sun *et al.* carried out a recyclability test. Pt_1-Co_1/CN has good photodegradation stability. After the reaction, the sample still maintained the crystal structure, which further demonstrated the recyclability of the sample.[142]

The stability of the performance and the stability of the structure are mutually restricted, which determines the stability of the material. The good stability enables the catalyst to continue to maintain its high efficiency in the long-running process.

8.3 Toxicity resistance of catalysts

The performance indexes of catalyst evaluation mainly include activity, selectivity, and stability. However, the catalyst may be deactivated due to some factors during use. One of the most important factors is catalyst poisoning. For example, common sulfides, chlorides, *etc.*, can poison the catalyst and inactivate it. Therefore, we need to improve the anti-poisoning performance of the catalyst.

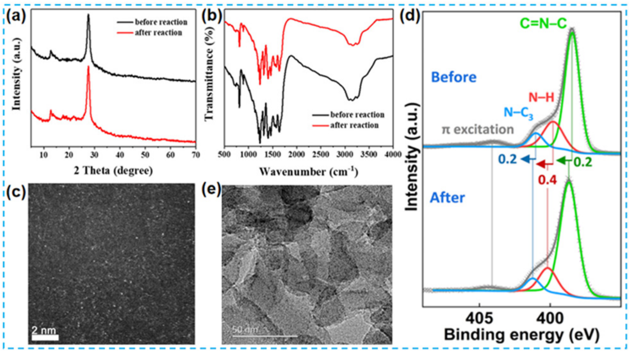

Fig. 30 (a) XRD and (b) FT-IR patterns of CoNiSx-CN before and after the photocatalytic H_2 evolution reaction.[118] (c) The spherical aberration-corrected HAADF-STEM image of Ce-SA-C_3N_4 after the photocatalytic hydrogen evolution from water splitting cycle experiments.[99] (d) N 1s core-level XPS spectra of W-PCN600 before and after the cyclic OWS experiment.[128] (e) TEM image of PtSA-CN620 after the photocatalytic H_2 production reaction.[129]

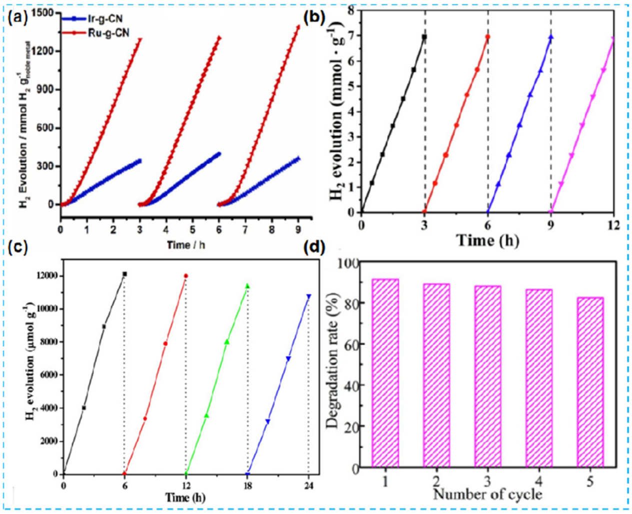

Fig. 31 (a) Photocatalytic test cycles of Ir-g-CN and Ru-g-CN under light irradiation.[64] (b) Cycling tests of the photocatalytic hydrogen evolution of 1.0%-Pt/CN-BH-H.[127] (c) Photocatalytic H_2-production of 24 h on the NiSCN5 photocatalyst with evacuation every 6 h.[117] (d) TC degradation efficiency over five cycles.[135]

Jiang *et al.* used a copolymerization strategy to synthesize CN-based catalysts with isolated Fe sites (Fig. 32a). The coordination mode of Fe–N_4 is conducive to the adsorption and activation of O_2 and H_2S. More importantly, the Fe based catalyst has the ability to

Table 3 Representative summary of H_2O_2 production by photocatalytic reduction using CN under visible light

Photocatalyst	Light source	Degradation/H_2O_2	Ref.
K^+/Na^+-g-C_3N_4	400–800 nm 250 W High-pressure sodium lamp	4.6 mmol L^{-1}	35
ACNN	λ > 420 nm (Xe)	10.2 mmol $h^{-1}g^{-1}$	37
Cu@mpg-C_3N_4	LED	Degradation of gemfibrozil: 3.3 fold	139
FeMn-C_3N_4	30 W LED light	Degradation of RhB: 8.0 fold	109
KNiCN	λ > 420 nm	79.6 μM	140
NiCN-4	λ > 420 nm (Xe)	27.11 mmol g^{-1} h^{-1}	77
CNR-0.5	5 W white LED light	2225.05 μmol^{-1} g^{-1}	36
Al-C_3N_4	AM 1.5	27.5 mmol g^{-1} h^{-1}	101
CNK	100 mW cm^{-2}	26.7 mmol g^{-1} h^{-1}	34

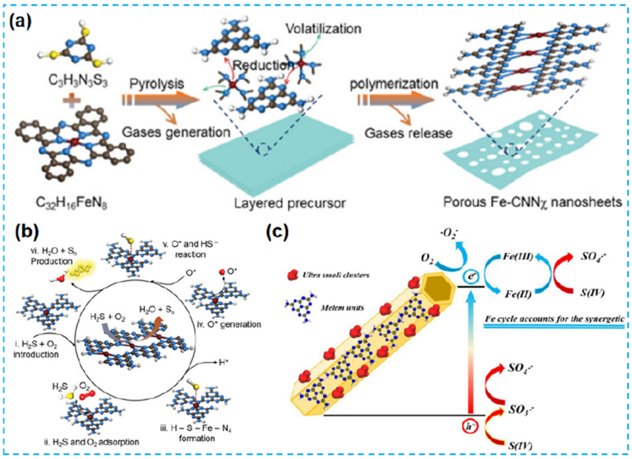

Fig. 32 (a) Fabrication scheme of Fe-CNNχ. (b) Catalytic reaction mechanism of H_2S selective oxidation on Fe-CNNχ.[143] (c) Schematic illustration of mechanisms for S(IV) activation by MF2 under visible light irradiation.[70]

resist sulfur poisoning (Fig. 32b).[143] Some natural products of diclofenac (DCF) have been reported to be more toxic than their parent molecules. Tong *et al.* used a supramolecular gel-assisted method to synthesize CN materials deposited with single atomic Fe and used photocatalysis technology to effectively remove DCF. The work reveals that dechlorination is the main detoxification mechanism (Fig. 32c).[70]

In recent years, CN-based catalysts doped with metals were investigated for the study of anti-poisoning properties of materials, and their application in electrocatalysis or thermal catalysis. For example, the prepared Rh-CN electrocatalyst is used in methanol oxidation.[144,145] The Ni in Ni-CN gives CN a new active site for hydrogen adsorption and activation, while physically isolating itself from the reaction environment and preventing poisoning or poisoning.[146] According to the current research situation, in future research, we should pay more attention to the preparation of all-in-one photocatalysts with high toxicity resistance. We should be committed to applying photocatalysis technology to a wider range of fields.

9 Conclusion and outlook

In this review, the latest research progress of metal-doped carbon nitride-based photocatalysts is summarized systematically. According to the periodic table of elements, alkali metal element doping, single metal atom (precious and non-precious metal) doping, and bimetal atom (precious and non-precious metal) doping are summarized. We found that pyrolysis and chemical reduction are the most common methods for anchoring metal atoms. Alkali metal doping mostly exists in the form of ions. The photocatalytic activity of the precious metal is enhanced by its excellent chemical properties in both single-atom doping and diatomic loading. These unique synthesis strategies and the enhancement of HER, CO_2 reduction, and H_2O_2 generation activities provide different ideas for subsequent researchers to construct novel and efficient metal-doped CN-based photocatalysts.

The research results of metal doping in photocatalysis have been systematically summarized in the third section. However, the research of CN-based photocatalysts modified by metal doping (especially bimetallic atom doping) is still in the initial stage. Therefore, the challenges and prospects for the subsequent preparation and application of photocatalysts are presented as follows:

(1) The light absorption range of the CN-based photocatalytic material is low (band gap width is 2.7 eV), and the photogenerated carrier is easy to recombine on the surface or in the bulk phase. Metal atoms are chemically bonded with CN to form an all-in-one photocatalyst. Therefore, the most critical research is to design and synthesize photocatalysts with a high absorption range and easy separation of photon-generated carriers. Metal atom and N coordination can act as a bridge of charge transfer between the atom and carrier, promoting the separation of photogenerated charges. Therefore, it is necessary to deeply understand and study multifunctional photocatalysts.

(2) The modification strategy of metal doping is conducive to anchoring N atoms in the CN cavity. If the metal can be loaded on CN in a single atomic state, the catalytic performance is improved while the atomic utilization is significantly improved. Therefore, how to prepare small-size photocatalysts with high loads is a topic worthy of further study.

(3) In addition to single-atom doping, diatomic doping is gradually attracting the attention of researchers because of its advantages such as a large active site, multiple reactions that can occur at the same time, and synergistic effect between two atoms. However, in recent years, the research on the diatomic modification of carbon-based materials and their application in photocatalysis has still been in the initial stage. The study of diatomic modification strategy is the key to synthesizing high-performance catalysts.

(4) The most widespread application of metal-modified CN materials is still photocatalytic hydrogen production, which can reach the order of millimolar. It is reported that Cu modified CN materials are widely used for carbon dioxide emission reduction. Therefore, the synthesis of multi-purpose and highly selective catalysts is worthy of in-depth study by researchers.

(5) The research on the anti-toxicity of metal-doped CN-based materials found that the use of photocatalysis technology to study anti-toxicity is rare. In future research, it is also necessary to focus on the anti-poisoning ability of the material. This is expected to be achieved by optimizing the metal loading capacity or adding a co-catalyst.

It is believed that the CN-based all-in-one photocatalyst doped with metals will shine in the field of photocatalysis and make outstanding contributions to solving the future global energy and environmental crisis.

Conflicts of interest

The authors declare no competing interests.

Acknowledgements

This study was financially supported by the National Natural Science Foundation of China (grant no. 22272003), the Key

Project of the National Natural Science Foundation of China (21936001 and 21801092), the Beijing Outstanding Young Scientists Program (BJJWZYJH01201910005017), the Beijing Natural Science Foundation (grant no. 2192005), and the Beijing Municipal Science and Natural Science Fund Project (grant no. KM201910005016).

References

1 S. Ye, R. Wang, M.-Z. Wu and Y.-P. Yuan, *Appl. Surf. Sci.*, 2015, **358**, 15–27.
2 Y. Zheng, L. Lin, B. Wang and X. Wang, *Angew. Chem., Int. Ed.*, 2015, **54**, 12868–12884.
3 X. Wang, K. Maeda, A. Thomas, K. Takanabe, G. Xin, J. M. Carlsson, K. Domen and M. Antonietti, *Nat. Mater.*, 2009, **8**, 76–80.
4 T. Xiong, W. Cen, Y. Zhang and F. Dong, *ACS Catal.*, 2016, **6**, 2462–2472.
5 Q. Han, B. Wang, J. Gao, Z. Cheng, Y. Zhao, Z. Zhang and L. Qu, *ACS Nano*, 2016, **10**, 2745–2751.
6 Y. Kang, Y. Yang, L. C. Yin, X. Kang, L. Wang, G. Liu and H. M. Cheng, *Adv. Mater.*, 2016, **28**, 6471–6477.
7 Y. Chen, F. Su, H. Xie, R. Wang, C. Ding, J. Huang, Y. Xu and L. Ye, *Chem. Eng. J.*, 2021, **404**, 126498.
8 V. W.-h Lau, V. W.-z Yu, F. Ehrat, T. Botari, I. Moudrakovski, T. Simon, V. Duppel, E. Medina, J. K. Stolarczyk, J. Feldmann, V. Blum and B. V. Lotsch, *Adv. Energy Mater.*, 2017, **7**, 1602251.
9 C. Ye, X. Wang, J. Li, Z. Li, X. Li, L. Zhang, B. Chen, C. Tung and L. Wu, *ACS Catal.*, 2016, **6**, 8336–8341.
10 Z. Mo, J. Di, P. Yan, C. Lv, X. Zhu, D. Liu, Y. Song, C. Liu, Q. Yu, H. Li, Y. Lei, H. Xu and Q. Yan, *Small*, 2020, **16**, 2003914.
11 P. Huang, J. Huang, S. A. Pantovich, A. D. Carl, T. G. Fenton, C. A. Caputo, R. L. Grimm, A. I. Frenkel and G. Li, *J. Am. Chem. Soc.*, 2018, **140**, 16042–16047.
12 Y. Ye, C. Wen, J. Pan, J. Wang, Y. Tong, S. Wei, Z. Ke, L. Jiang, F. Zhu, N. Zhou, M. Zhou, J. Xu and G. Ouyang, *Appl. Catal., B*, 2021, **285**, 119726.
13 W. Wang, H. Zhang, S. Zhang, Y. Liu, G. Wang, C. Sun and H. Zhao, *Angew. Chem., Int. Ed.*, 2019, **58**, 16644–16650.
14 X. Jia, J. Zhao, Y. Lv, X. Fu, Y. Jian, W. Zhang, Y. Wang, H. Sun, X. Wang, J. Long, P. Yang, Q. Gu and Z. Gao, *Appl. Catal., B*, 2022, **300**, 120756.
15 B. Li, Y. Si, B. X. Zhou, Q. Fang, Y. Y. Li, W. Q. Huang, W. Hu, A. Pan, X. Fan and G. F. Huang, *ACS Appl. Mater. Interfaces*, 2019, **11**, 17341–17349.
16 X. Wu, H. Fan, W. Wang, L. Lei, X. Chang and L. Ma, *J. Mater. Chem. A*, 2022, **10**, 17817–17826.
17 Y. Han, X. Lu, S. Tang, X. Yin, Z. Wei and T. Lu, *Adv. Energy Mater.*, 2018, **8**, 1702992.
18 Z. Zhang, R. Ji, Q. Sun, J. He, D. Chen, N. Li, H. Li, A. Marcomini, Q. Xu and J. Lu, *Appl. Catal., B*, 2023, **324**, 122276.
19 Y. Lin, W. Su, X. Wang, X. Fu and X. Wang, *Angew. Chem., Int. Ed.*, 2020, **59**, 20919–20923.
20 D. Zhao, Y. Wang, C. Dong, Y. Huang, J. Chen, F. Xue, S. Shen and L. Guo, *Nat. Energy*, 2021, **6**, 388–397.
21 K. Li and W. D. Zhang, *Small*, 2018, **14**, 1703599.
22 A. Torres-Pinto, M. J. Sampaio, C. G. Silva, J. L. Faria and A. M. T. Silva, *Appl. Catal., B*, 2019, **252**, 128–137.
23 T. Zhang, W. Schilling, S. U. Khan, H. Y. V. Ching, C. Lu, J. Chen, A. Jaworski, G. Barcaro, S. Monti, K. De Wael, A. Slabon and S. Das, *ACS Catal.*, 2021, **11**, 14087–14101.
24 X. Fan, L. Zhang, R. Cheng, M. Wang, M. Li, Y. Zhou and J. Shi, *ACS Catal.*, 2015, **5**, 5008–5015.
25 Z. Ma, X. Zong, Q. Hong, L. Niu, T. Yang, W. Jiang, D. Qu, L. An, X. Wang, Z. Kang and Z. Sun, *Appl. Catal., B*, 2022, **319**, 121922.
26 V. W. Lau, I. Moudrakovski, T. Botari, S. Weinberger, M. B. Mesch, V. Duppel, J. Senker, V. Blum and B. V. Lotsch, *Nat. Commun.*, 2016, **7**, 12165–12175.
27 Z. Zhang, L. Lu, Z. Lv, Y. Chen, H. Jin, S. Hou, L. Qiu, L. Duan, J. Liu and K. Dai, *Appl. Catal., B*, 2018, **232**, 384–390.
28 B. Yue, Q. Li, H. Iwai, T. Kako and J. Ye, *Sci. Technol. Adv. Mater.*, 2011, **12**, 034401.
29 Q. Zhang, J. Chen, H. Che, P. Wang, B. Liu and Y. Ao, *ACS Mater. Lett.*, 2022, **4**, 2166–2186.
30 C. Tang, M. Cheng, C. Lai, L. Li, X. Yang, L. Du, G. Zhang, G. Wang and L. Yang, *Coord. Chem. Rev.*, 2023, **474**, 214846.
31 S. Hu, F. Li, Z. Fan, F. Wang, Y. Zhao and Z. Lv, *Dalton Trans.*, 2015, **44**, 1084–1092.
32 J. Tang, K. W. Kemp, S. Hoogland, K. S. Jeong, H. Liu, L. Levina, M. Furukawa, X. Wang, R. Debnath, D. Cha, K. W. Chou, A. Fischer, A. Amassian, J. B. Asbury and E. H. Sargent, *Nat. Mater.*, 2011, **10**, 765–771.
33 Y. Wang, S. Zhao, Y. Zhang, J. Fang, Y. Zhou, S. Yuan, C. Zhang and W. Chen, *Appl. Surf. Sci.*, 2018, **440**, 258–265.
34 Z. Yang, L. Li, S. Zeng, J. Cui, K. Wang, C. Hu and Y. Zhao, *ACS Appl. Mater. Interfaces*, 2023, **15**, 8232–8240.
35 X. Qu, S. Hu, J. Bai, P. Li, G. Lu and X. Kang, *J. Mater. Sci. Technol.*, 2018, **34**, 1932–1938.
36 Z. Li, T. Chen, Y. Chen, X. Chen, L. Li, S. Kuang, J. Gao, Y. Guo, T. W. Benedict Lo and J. Du, *J. Mater. Chem. A*, 2023, **11**, 5925–5936.
37 S. Wu, H. Yu, S. Chen and X. Quan, *ACS Catal.*, 2020, **10**, 14380–14389.
38 M. Cui, K. Cui, X. Liu, X. Chen, Y. Chen and Z. Guo, *J. Hazard. Mater.*, 2022, **424**, 127292.
39 H. Dong, M. Xiao, S. Yu, H. Wu, Y. Wang, J. Sun, G. Chen and C. Li, *ACS Catal.*, 2019, **10**, 458–462.
40 B. Qiao, A. Wang, X. Yang, L. F. Allard, Z. Jiang, Y. Cui, J. Liu, J. Li and T. Zhang, *Nat. Chem.*, 2011, **3**, 634–641.
41 X. Li, W. Bi, L. Zhang, S. Tao, W. Chu, Q. Zhang, Y. Luo, C. Wu and Y. Xie, *Adv. Mater.*, 2016, **28**, 2427–2431.
42 Y. Zhu, T. Wang, T. Xu, Y. Li and C. Wang, *Appl. Surf. Sci.*, 2019, **464**, 36–42.
43 B. Lin, H. An, X. Yan, T. Zhang, J. Wei and G. Yang, *Appl. Catal., B*, 2017, **210**, 173–183.

44 Y. Hu, Y. Qu, Y. Zhou, Z. Wang, H. Wang, B. Yang, Z. Yu and Y. Wu, *Chem. Eng. J.*, 2021, **412**, 129749.

45 X. Liu, S. Wang, W. Yu, J. Zhang, S. Fang, J. Zhang, J. Qiu, F. Kong and X. Duan, *Chem. Eng. J.*, 2022, **446**, 137426.

46 X. Shi, Y. Huang, Y. Bo, D. Duan, Z. Wang, J. Cao, G. Zhu, W. Ho, L. Wang, T. Huang and Y. Xiong, *Angew. Chem., Int. Ed.*, 2022, **61**, e202203063.

47 L. Zhang, R. Long, Y. Zhang, D. Duan, Y. Xiong, Y. Zhang and Y. Bi, *Angew. Chem., Int. Ed.*, 2020, **59**, 6224–6229.

48 Z. Zeng, F. Ye, S. Deng, D. Fang, X. Wang, Y. Bai and H. Xiao, *Chem. Eng. J.*, 2022, **444**, 136561.

49 Z. Zeng, Y. Su, X. Quan, W. Choi, G. Zhang, N. Liu, B. Kim, S. Chen, H. Yu and S. Zhang, *Nano Energy*, 2020, **69**, 104409.

50 J. Yan, Y. Ji, M. Batmunkh, P. An, J. Zhang, Y. Fu, B. Jia, Y. Li, S. Liu, J. Ye and T. Ma, *Angew. Chem., Int. Ed.*, 2021, **60**, 2541–2547.

51 S. Cao, H. Li, T. Tong, H. Chen, A. Yu, J. Yu and H. M. Chen, *Adv. Funct. Mater.*, 2018, **28**, 1802169.

52 M. Ren, X. Zhang, Y. Liu, G. Yang, L. Qin, J. Meng, Y. Guo and Y. Yang, *ACS Catal.*, 2022, **12**, 5077–5093.

53 M. Gao, F. Tian, X. Zhang, Y. Liu, Z. Chen, Y. Yu, W. Yang and Y. Hou, *Nano Energy*, 2022, **103**, 107767.

54 G. Vile, D. Albani, M. Nachtegaal, Z. Chen, D. Dontsova, M. Antonietti, N. Lopez and J. Perez-Ramirez, *Angew. Chem., Int. Ed.*, 2015, **54**, 11265–11269.

55 K. Fujiwara and S. E. Pratsinis, *Appl. Catal., B*, 2018, **226**, 127–134.

56 G. Liu, Y. Huang, H. Lv, H. Wang, Y. Zeng, M. Yuan, Q. Meng and C. Wang, *Appl. Catal., B*, 2021, **284**, 119683.

57 L. Hu, T. Wang, Q. Nie, J. Liu, Y. Cui, K. Zhang, Z. Tan and H. Yu, *Carbon*, 2022, **200**, 187–198.

58 X. H. Jiang, L. S. Zhang, H. Y. Liu, D. S. Wu, F. Y. Wu, L. Tian, L. L. Liu, J. P. Zou, S. L. Luo and B. B. Chen, *Angew. Chem., Int. Ed.*, 2020, **59**, 23112–23116.

59 B. Yan, Y. He and G. Yang, *Small*, 2022, **18**, e2107840.

60 B. Yan, H. Song and G. Yang, *Chem. Eng. J.*, 2022, **427**, 24217–24221.

61 L. Zeng, C. Dai, B. Liu and C. Xue, *J. Mater. Chem. A*, 2019, **7**, 24217–24221.

62 P. Sharma, S. Kumar, O. Tomanec, M. Petr, J. Zhu Chen, J. T. Miller, R. S. Varma, M. B. Gawande and R. Zboril, *Small*, 2021, **17**, e2006478.

63 J. Deng, C. Zhou, Y. Yang, B. Nan, L. Dong, L. Cai, L. Li, Z. Wang, X. Yang and Z. Chen, *Chem. Eng. J.*, 2023, **462**, 142282.

64 Z. Yu, Y. Li, A. Torres-Pinto, A. P. LaGrow, V. M. Diaconescu, L. Simonelli, M. J. Sampaio, O. Bondarchuk, I. Amorim, A. Araujo, A. M. T. Silva, C. G. Silva, J. L. Faria and L. Liu, *Appl. Catal., B*, 2022, **310**, 121318.

65 Y. Yin, L. Shi, W. Li, X. Li, H. Wu, Z. Ao, W. Tian, S. Liu, S. Wang and H. Sun, *Environ. Sci. Technol.*, 2019, **53**, 11391–11400.

66 S. An, G. Zhang, T. Wang, W. Zhang, K. Li, C. Song, J. T. Miller, S. Miao, J. Wang and X. Guo, *ACS Nano*, 2018, **12**, 9441–9450.

67 G. Zhao, W. Li, H. Zhang, W. Wang and Y. Ren, *Chem. Eng. J.*, 2022, **430**, 132937.

68 S. Liu, D. Liu, Y. Sun, P. Xiao, H. Lin, J. Chen, X. Wu, X. Duan and S. Wang, *Appl. Catal., B*, 2022, **310**, 121327.

69 X. Xiao, Z. Ruan, Q. Li, L. Zhang, H. Meng, Q. Zhang, H. Bao, B. Jiang, J. Zhou, C. Guo, X. Wang and H. Fu, *Adv. Mater.*, 2022, **34**, e2200612.

70 Z. Zhao, W. Zhang, W. Liu, Y. Li, J. Ye, J. Liang and M. Tong, *Chem. Eng. J.*, 2021, **407**, 127167.

71 L. Su, P. Wang, X. Ma, J. Wang and S. Zhan, *Angew. Chem., Int. Ed.*, 2021, **60**, 21261–21266.

72 G. Wang, Y. Ma, T. Zhang, Y. Liu, B. Wang, R. Zhang and Z. Zhao, *Small*, 2023, **19**, e2205758.

73 Y. Huang, Y. Jian, L. Li, D. Li, Z. Fang, W. Dong, Y. Lu, B. Luo, R. Chen, Y. Yang, M. Chen and W. Shi, *Angew. Chem., Int. Ed.*, 2021, **60**, 5245–5249.

74 L. Hu, J. Huang, J. Wang, S. Jiang, C. Sun and S. Song, *Appl. Catal., B*, 2023, **320**, 121945.

75 L. Cheng, H. Yin, C. Cai, J. Fan and Q. Xiang, *Small*, 2020, **16**, e2002411.

76 X. Song, N. Li, H. Zhang, L. Wang, Y. Yan, H. Wang, L. Wang and Z. Bian, *ACS Appl. Mater. Interfaces*, 2020, **12**, 17519–17527.

77 Y.-Z. Zhang, C. Liang, H.-P. Feng and W. Liu, *Chem. Eng. J.*, 2022, **446**, 137379.

78 G. Han, Y. H. Jin, R. A. Burgess, N. E. Dickenson, X. M. Cao and Y. Sun, *J. Am. Chem. Soc.*, 2017, **139**, 15584–15587.

79 Q. Lin, Y.-H. Li, M.-Y. Qi, J.-Y. Li, Z.-R. Tang, M. Anpo, Y. M. A. Yamada and Y.-J. Xu, *Appl. Catal., B*, 2020, **271**, 118946.

80 X. Jin, R. Wang, L. Zhang, R. Si, M. Shen, M. Wang, J. Tian and J. Shi, *Angew. Chem., Int. Ed.*, 2020, **59**, 6827–6831.

81 D. K. Chauhan, V. R. Battula, S. Jain and K. Kailasam, *J. Cleaner Prod.*, 2021, **307**, 127162.

82 A. Vijeta, C. Casadevall, S. Roy and E. Reisner, *Angew. Chem., Int. Ed.*, 2021, **60**, 8494–8499.

83 A. Vijeta, C. Casadevall and E. Reisner, *Angew. Chem., Int. Ed.*, 2022, **61**, e202203176.

84 J. Ma, F. Zhang, Y. Tan, S. Wang, H. Chen, L. Zheng, H. Liu and R. Li, *ACS Appl. Mater. Interfaces*, 2022, **14**, 18383–18392.

85 M. Kwak, J. Bok, B. H. Lee, J. Kim, Y. Seo, S. Kim, H. Choi, W. Ko, W. Hooch Antink, C. W. Lee, G. H. Yim, H. Seung, C. Park, K. S. Lee, D. H. Kim, T. Hyeon and D. Yoo, *Chem. Sci.*, 2022, **13**, 8536–8542.

86 T. Jia, D. Meng, R. Duan, H. Ji, H. Sheng, C. Chen, J. Li, W. Song and J. Zhao, *Angew. Chem., Int. Ed.*, 2023, **62**, e202216511.

87 X. Sun, L. Sun, G. Li, Y. Tuo, C. Ye, J. Yang, J. Low, X. Yu, J. H. Bitter, Y. Lei, D. Wang and Y. Li, *Angew. Chem., Int. Ed.*, 2022, **61**, e202207677.

88 Y. Zhou, L. Zhang and W. Wang, *Nat. Commun.*, 2019, **10**, 506–514.

89 X. Xiao, Y. Gao, L. Zhang, J. Zhang, Q. Zhang, Q. Li, H. Bao, J. Zhou, S. Miao, N. Chen, J. Wang, B. Jiang, C. Tian and H. Fu, *Adv. Mater.*, 2020, **32**, e2003082.

90 T. Zhang, Z. Sun, S. Li, B. Wang, Y. Liu, R. Zhang and Z. Zhao, *Nat. Commun.*, 2022, **13**, 6996–7004.

91 C. Han, R. Qi, R. Sun, K. Fan, B. Johannessen, D. Qi, S. Cao and J. Xu, *Appl. Catal., B*, 2023, **320**, 121954.

92 Y. Li, B. Li, D. Zhang, L. Cheng and Q. Xiang, *ACS Nano*, 2020, **14**, 10552–10561.

93 D. Zhao, Y. Wang, C. L. Dong, F. Meng, Y. C. Huang, Q. Zhang, L. Gu, L. Liu and S. Shen, *Nanomicro Lett.*, 2022, **14**, 223–238.

94 R. Zhang, Y. Cao, D. E. Doronkin, M. Ma, F. Dong and Y. Zhou, *Chem. Eng. J.*, 2023, **454**, 140084.

95 B. Xu, X. Fu, X. You, E. Zhao, F. Li, Z. Chen, Y. Li, X. Wang and Y. Yao, *ACS Catal.*, 2022, **12**, 6958–6967.

96 R. Zhang, P. Li, F. Wang, L. Ye, A. Gaur, Z. Huang, Z. Zhao, Y. Bai and Y. Zhou, *Appl. Catal., B*, 2019, **250**, 273–279.

97 J. Luo, H. Han, X. Wang, X. Qiu, B. Liu, Y. Lai, X. Chen, R. Zhong, L. Wang and C. Wang, *Appl. Catal., B*, 2023, **328**, 122495.

98 P. Chen, B. Lei, X. Dong, H. Wang, J. Sheng, W. Cui, J. Li, Y. Sun, Z. Wang and F. Dong, *ACS Nano*, 2020, **14**, 15841–15852.

99 D. Sun, Y. Chen, X. Yu, Y. Yin and G. Tian, *Chem. Eng. J.*, 2023, **462**, 142084.

100 W. Jiang, Y. Zhao, X. Zong, H. Nie, L. Niu, L. An, D. Qu, X. Wang, Z. Kang and Z. Sun, *Angew. Chem., Int. Ed.*, 2021, **60**, 6124–6129.

101 C. Zhuang, W. Li, T. Zhang, J. Li, Y. Zhang, G. Chen, H. Li, Z. Kang, J. Zou and X. Han, *Nano Energy*, 2023, **108**, 108225.

102 G. Sun, Z. J. Zhao, R. Mu, S. Zha, L. Li, S. Chen, K. Zang, J. Luo, Z. Li, S. C. Purdy, A. J. Kropf, J. T. Miller, L. Zeng and J. Gong, *Nat. Commun.*, 2018, **9**, 4454–4463.

103 S. Chen, B. Gong, J. Gu, Y. Lin, B. Yang, Q. Gu, R. Jin, Q. Liu, W. Ying, X. Shi, W. Xu, L. Cai, Y. Li, Z. Sun, S. Wei, W. Zhang and J. Lu, *Angew. Chem., Int. Ed.*, 2022, **61**, e202211919.

104 L. Cheng, X. Yue, L. Wang, D. Zhang, P. Zhang, J. Fan and Q. Xiang, *Adv. Mater.*, 2021, **33**, e2105135.

105 L. Cheng, P. Zhang, Q. Wen, J. Fan and Q. Xiang, *Chin. J. Catal.*, 2022, **43**, 451–460.

106 M. Yu, C. Liu, X. Sun, J. Lu and J. Niu, *ACS Appl. Mater. Interfaces*, 2022, **14**, 5376–5383.

107 Z. Wu, Z. Tong, Y. Xie, H. Sun, X. Gong, P. Qin, Y. Liang, X. Yuan, D. Zou and L. Jiang, *Chem. Eng. J.*, 2022, **434**, 134732.

108 Y. Gu, Z. Zhou, Z. Lin, X. Liu, T. Xu, W. Chen and W. Lu, *Chem. Eng. J.*, 2023, **455**, 140759.

109 Z. Huang, M. Shen, J. Liu, J. Ye and T. Asefa, *J. Mater. Chem. A*, 2021, **9**, 14841–14850.

110 H. Ou, S. Ning, P. Zhu, S. Chen, A. Han, Q. Kang, Z. Hu, J. Ye, D. Wang and Y. Li, *Angew. Chem., Int. Ed.*, 2022, **61**, e202206579.

111 W. Wu, Z. Ruan, J. Li, Y. Li, Y. Jiang, X. Xu, D. Li, Y. Yuan and K. Lin, *Nanomicro Lett.*, 2019, **11**, 10–26.

112 L. Li, H. Guo, G. Yao, C. Hu, C. Liu, Z. Tian, B. Li, Q. Zhang and L. Chen, *J. Mater. Chem. A*, 2020, **8**, 22327–22334.

113 H. Shi, H. Wang, Y. Zhou, J. Li, P. Zhai, X. Li, G. G. Gurzadyan, J. Hou, H. Yang and X. Guo, *Angew. Chem., Int. Ed.*, 2022, **61**, e202208904.

114 H. Shi, J. Li, H. Wang, J. Hou, K. Li and X. Guo, *Appl. Catal., B*, 2023, **322**, 122139.

115 B. Kim, D. Kwon, J. O. Baeg, M. Austeria P, G. H. Gu, J. H. Lee, J. Jeong, W. Kim and W. Choi, *Adv. Funct. Mater.*, 2023, **33**, 2212453.

116 Y. Guo, Q. Liu, Z. Li, Z. Zhang and X. Fang, *Appl. Catal., B*, 2018, **221**, 362–370.

117 C. Sun, H. Zhang, H. Liu, X. Zheng, W. Zou, L. Dong and L. Qi, *Appl. Catal., B*, 2018, **235**, 66–74.

118 L. Jiang, K. Wang, X. Wu, G. Zhang and S. Yin, *ACS Appl. Mater. Interfaces*, 2019, **11**, 26898–26908.

119 P. Deng, J. Xiong, S. Lei, W. Wang, X. Ou, Y. Xu, Y. Xiao and B. Cheng, *J. Mater. Chem. A*, 2019, **7**, 22385–22397.

120 Z. Jin and L. Zhang, *J. Mater. Sci. Technol.*, 2020, **49**, 144–156.

121 L. Chen, D. Zhu, J. Li, X. Wang, J. Zhu, P. S. Francis and Y. Zheng, *Appl. Catal., B*, 2020, **273**, 119050.

122 T. Lee, H. Kang, J. Kim, N. Suzuki, A. Fujishima, M. Choi and Y. Jun, *Appl. Catal., B*, 2021, **294**, 120222.

123 X. Yu, H. Su, J. Zou, Q. Liu, L. Wang and H. Tang, *Chin. J. Catal.*, 2022, **43**, 421–432.

124 Q. Mo, L. Zhang, S. Li, H. Song, Y. Fan and C. Y. Su, *J. Am. Chem. Soc.*, 2022, **144**, 22747–22758.

125 X. Zhang, X. Ran Zhang, P. Yang, H. Chen and S. Jiang, *Chem. Eng. J.*, 2022, **450**, 138030.

126 P. Chen, Q. Ruan, R. Nasseri, H. Zhang, X. Xi, H. Xia, G. Xu, Q. Xie, C. Yi, Z. Sun, H. Shahsavan and W. Zhang, *Adv. Sci.*, 2022, **9**, e2204730.

127 J. Wu, X. Xi, W. Zhu, Z. Yang, P. An, Y. Wang, Y. Li, Y. Zhu, W. Yao and G. Jiang, *Chem. Eng. J.*, 2022, **442**, 136334.

128 F. Yu, Q. Deng, H. Li, Y. Xia and W. Hou, *Appl. Catal., B*, 2023, **323**, 122180.

129 P. Zhou, F. Lv, N. Li, Y. Zhang, Z. Mu, Y. Tang, J. Lai, Y. Chao, M. Luo, F. Lin, J. Zhou, D. Su and S. Guo, *Nano Energy*, 2019, **56**, 127–137.

130 Z. Su, J. Zhang, Z. Tan, J. Hu, F. Zhang, R. Duan, L. Yao, B. Han, Y. Zhao and Y. Yang, *Green Chem.*, 2023, **25**, 2577–2582.

131 P. Liu, Z. Huang, X. Gao, X. Hong, J. Zhu, G. Wang, Y. Wu, J. Zeng and X. Zheng, *Adv. Mater.*, 2022, **34**, e2200057.

132 G. Wang, Z. Chen, T. Wang, D. Wang and J. Mao, *Angew. Chem., Int. Ed.*, 2022, **61**, e202210789.

133 X. Cheng, J. Wang, K. Zhao and Y. Bi, *Appl. Catal., B*, 2022, **316**, 121643.

134 Z. Liu, J. Ma, M. Hong and R. Sun, *ACS Catal.*, 2023, **13**, 2106–2117.

135 J. Xu, Y. Chen, M. Chen, J. Wang and L. Wang, *Chem. Eng. J.*, 2022, **442**, 136208.

136 Q. Liu, J. Lin, H. Cheng, L. Wei and F. Wang, *Angew. Chem., Int. Ed.*, 2023, **62**, e202218720.

137 B. Kim, D. Kwon, J. O. Baeg, M. Austeria P, G. H. Gu, J. H. Lee, J. Jeong, W. Kim and W. Choi, *Adv. Funct. Mater.*, 2023, **33**, 2212453.

138 Y. Liu, J. Sun, H. Huang, L. Bai, X. Zhao, B. Qu, L. Xiong, F. Bai, J. Tang and L. Jing, *Nat. Commun.*, 2023, **14**, 1457–1468.

139 J. Liu, Y. Zou, D. Cruz, A. Savateev, M. Antonietti and G. Vile, *ACS Appl. Mater. Interfaces*, 2021, **13**, 25858–25867.

140 Y. Chen, X. Yan, J. Xu and L. Wang, *J. Mater. Chem. A*, 2021, **9**, 24056–24063.

141 B. Kim, D. Kwon, J. O. Baeg, M. Austeria P, G. Gu, J. Lee, J. Jeong, W. Kim and W. Choi, *Adv. Funct. Mater.*, 2023, **33**, 2212453.

142 M. Yang, J. Mei, Y. Ren, J. Cui, S. Liang and S. Sun, *J. Energy Chem.*, 2023, **81**, 502–509.

143 G. Lei, Y. Tong, L. Shen, F. Liu, Y. Xiao, W. Lin, Y. Zhang, C. Au and L. Jiang, *Small*, 2020, **16**, e2003904.

144 X. Du, W. Cai, Q. Zhang, L. Yang and H. He, *ACS Appl. Nano Mater.*, 2021, **4**, 9729–9737.

145 C. Li, Z. Wang, X. Sui, L. Zhang, D. Gu and S. Gu, *J. Mater. Chem. A*, 2014, **2**, 20139–20146.

146 T. Fu, M. Wang, W. Cai, Y. Cui, F. Gao, L. Peng, W. Chen and W. Ding, *ACS Catal.*, 2014, **4**, 2536–2543.